WJE ENGINEERS ARCHITECTS MATERIALS SCIENTISTS

APPENDIX A

Visual, Sounding, and Half-Cell Potential Plans

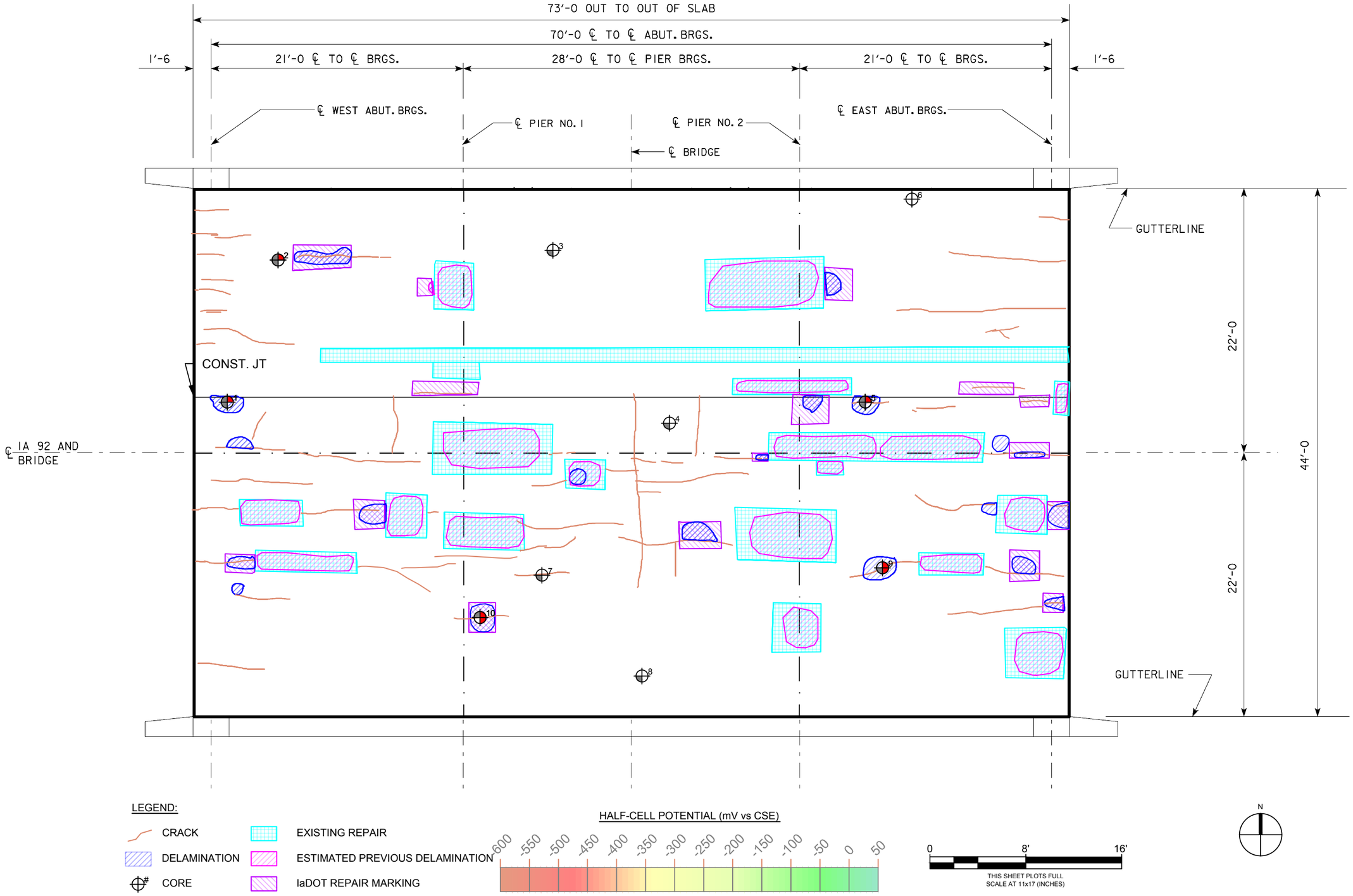
73'-0 OUT TO OUT OF SLAB
70'-0 ℄ TO ℄ ABUT. BRGS.
1'-6
21'-0 ℄ TO ℄ BRGS.
28'-0 ℄ TO ℄ PIER BRGS.
21'-0 ℄ TO ℄ BRGS.
1'-6
℄ WEST ABUT. BRGS.
℄ PIER NO. 1
℄ PIER NO. 2
℄ EAST ABUT. BRGS.
℄ BRIDGE
GUTTERLINE
22'-0
44'-0
CONST. JT
℄ IA 92 AND BRIDGE
GUTTERLINE
22'-0
LEGEND:
CRACK
DELAMINATION
CORE
EXISTING REPAIR
ESTIMATED PREVIOUS DELAMINATION
IaDOT REPAIR MARKING
HALF-CELL POTENTIAL (mV vs CSE)
-600 -550 -500 -450 -400 -350 -300 -250 -200 -150 -100 -50 0 50
0 8' 16'
THIS SHEET PLOTS FULL SCALE AT 11x17 (INCHES)
N

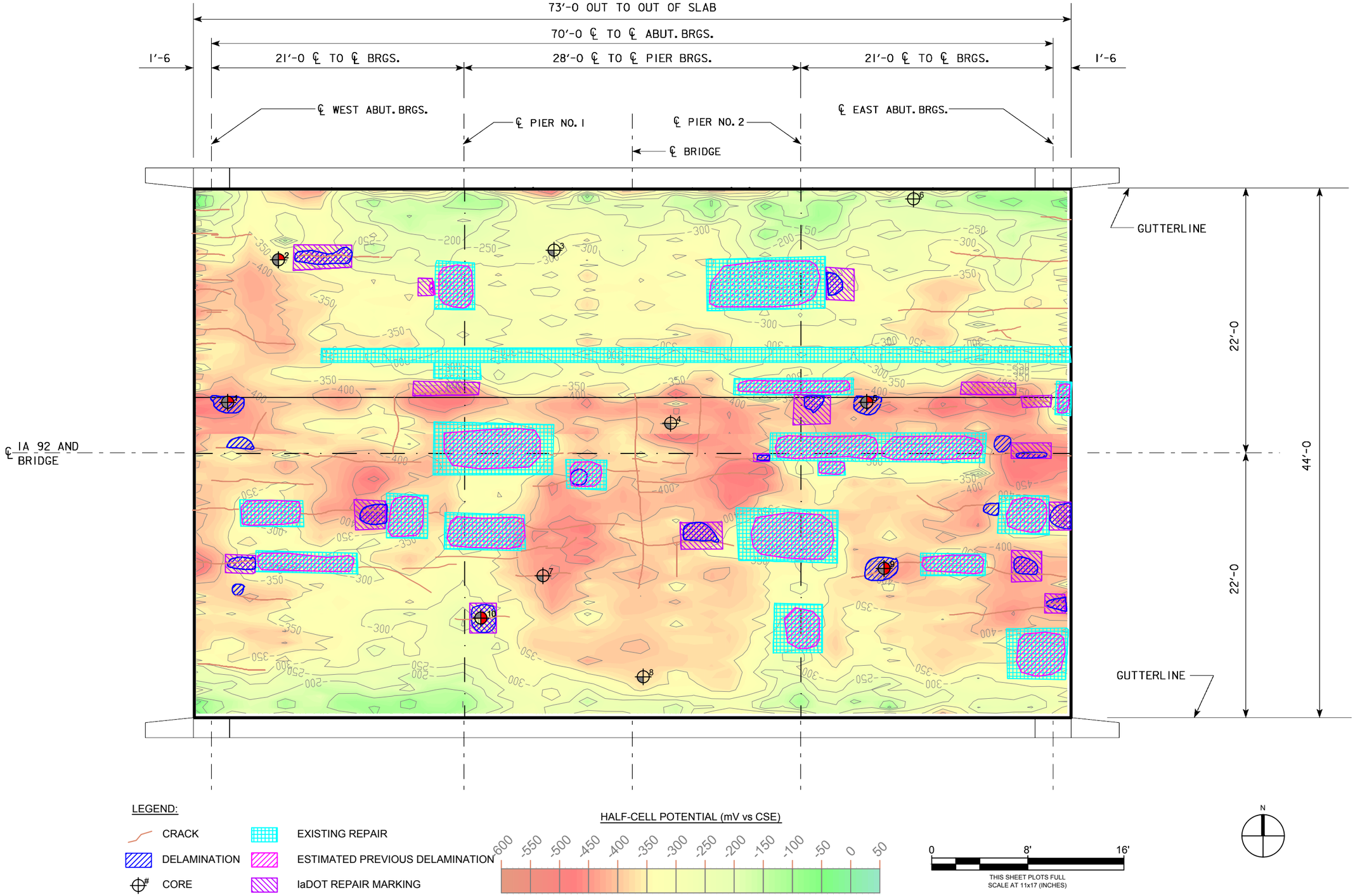
73'-0 OUT TO OUT OF SLAB
70'-0 ℄ TO ℄ ABUT. BRGS.
1'-6
21'-0 ℄ TO ℄ BRGS.
28'-0 ℄ TO ℄ PIER BRGS.
21'-0 ℄ TO ℄ BRGS.
1'-6
℄ WEST ABUT. BRGS.
℄ PIER NO. 1
℄ PIER NO. 2
℄ EAST ABUT. BRGS.
℄ BRIDGE
GUTTERLINE
22'-0
44'-0
℄ IA 92 AND BRIDGE
GUTTERLINE
LEGEND:
CRACK
DELAMINATION
CORE
EXISTING REPAIR
ESTIMATED PREVIOUS DELAMINATION
IaDOT REPAIR MARKING
HALF-CELL POTENTIAL (mV vs CSE)
-600 -550 -500 -450 -400 -350 -300 -250 -200 -150 -100 -50 0 50
0 8' 16'
THIS SHEET PLOTS FULL SCALE AT 11x17 (INCHES)
N

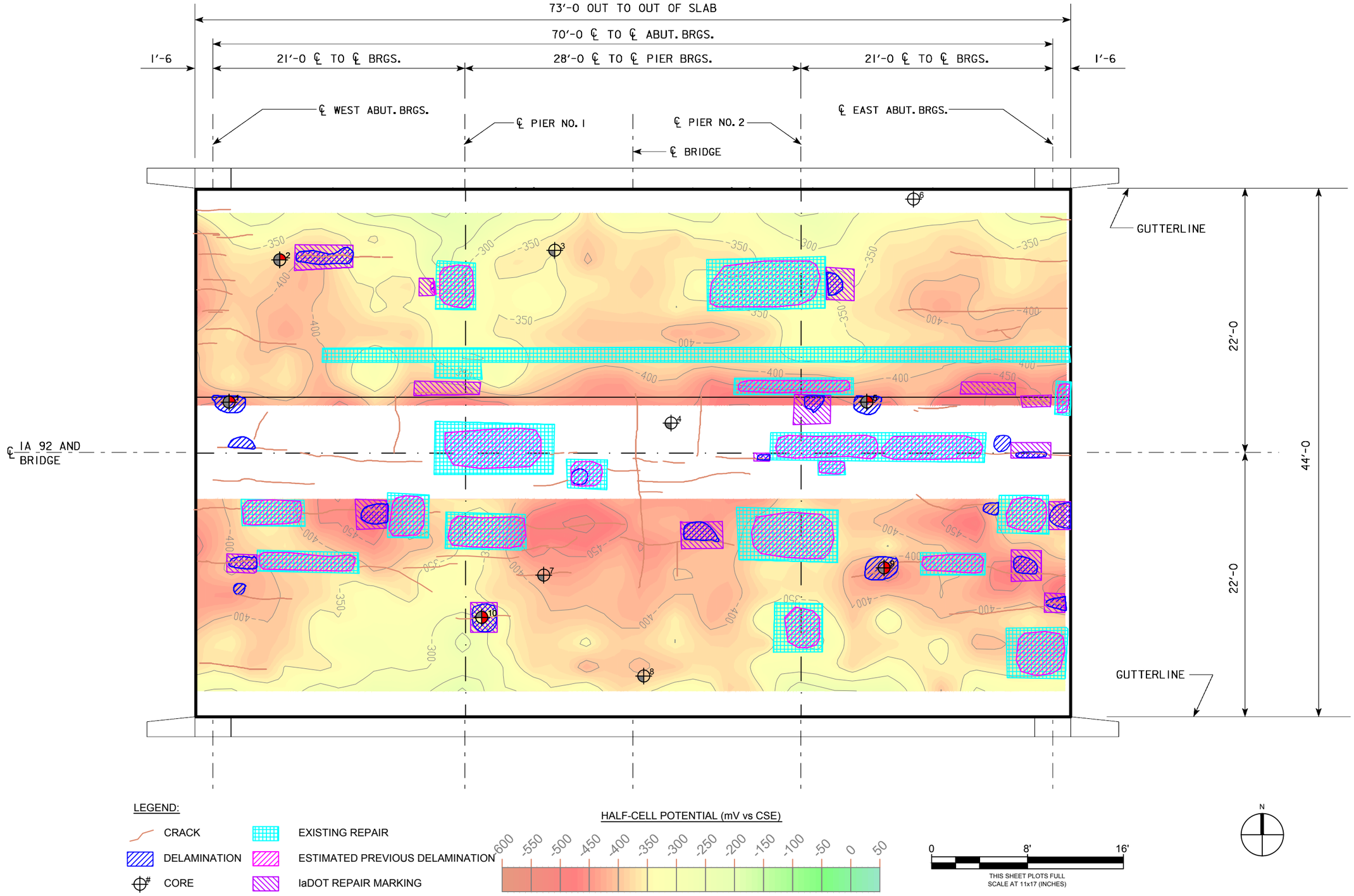
73'-0 OUT TO OUT OF SLAB
70'-0 ℄ TO ℄ ABUT. BRGS.
1'-6
21'-0 ℄ TO ℄ BRGS.
28'-0 ℄ TO ℄ PIER BRGS.
21'-0 ℄ TO ℄ BRGS.
1'-6
℄ WEST ABUT. BRGS.
℄ PIER NO. 1
℄ PIER NO. 2
℄ EAST ABUT. BRGS.
℄ BRIDGE
GUTTERLINE
22'-0
44'-0
℄ IA 92 AND BRIDGE
GUTTERLINE
LEGEND:
CRACK
DELAMINATION
CORE
EXISTING REPAIR
ESTIMATED PREVIOUS DELAMINATION
IaDOT REPAIR MARKING
HALF-CELL POTENTIAL (mV vs CSE)
-600 -550 -500 -450 -400 -350 -300 -250 -200 -150 -100 -50 0 50
0 8' 16'
THIS SHEET PLOTS FULL SCALE AT 11x17 (INCHES)
N

WJE ENGINEERS ARCHITECTS MATERIALS SCIENTISTS

APPENDIX B

Core Sample Photographs

Figure 1. Photographs of Core 1.

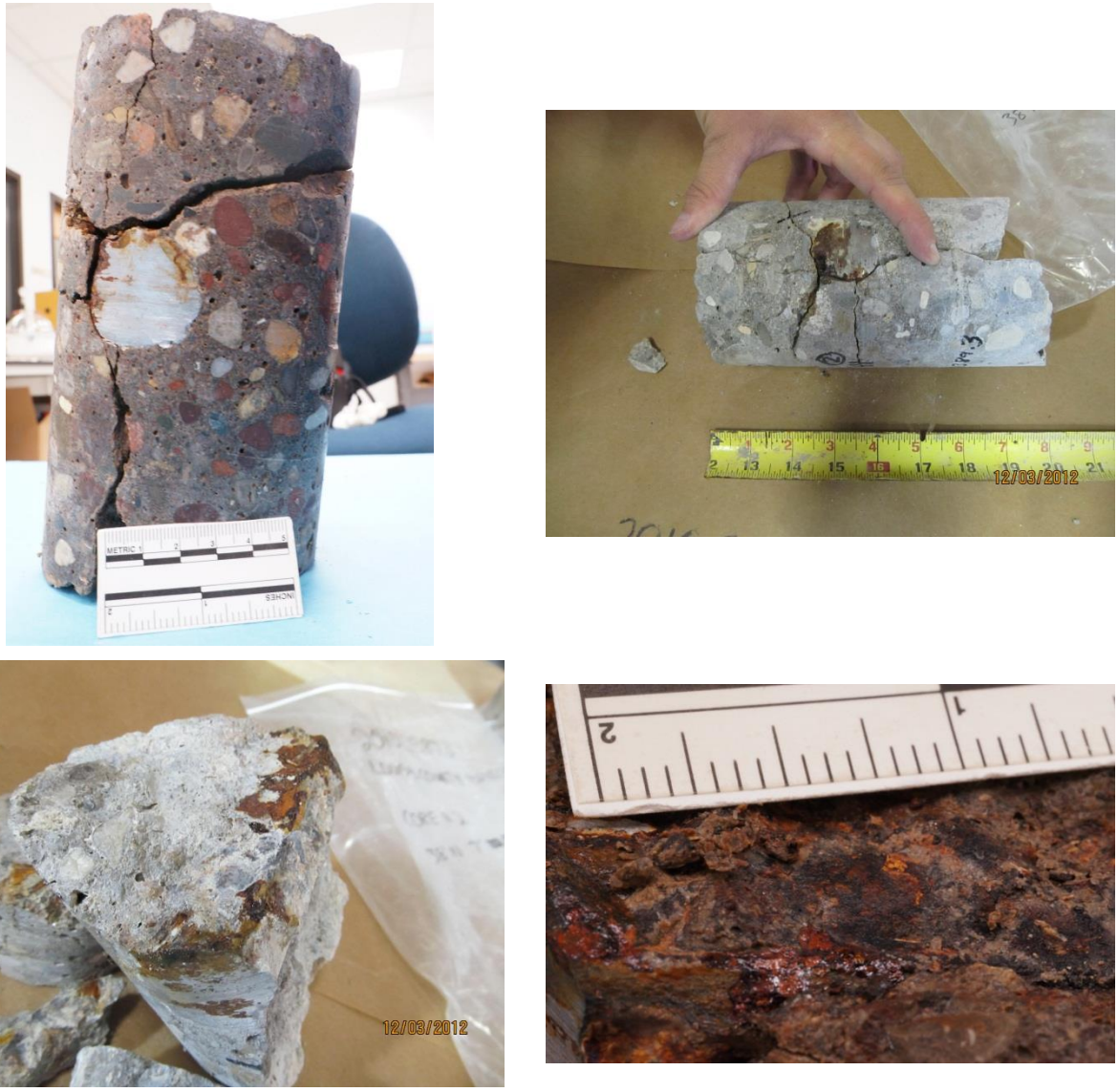

Figure 2. Photographs of Core 2.

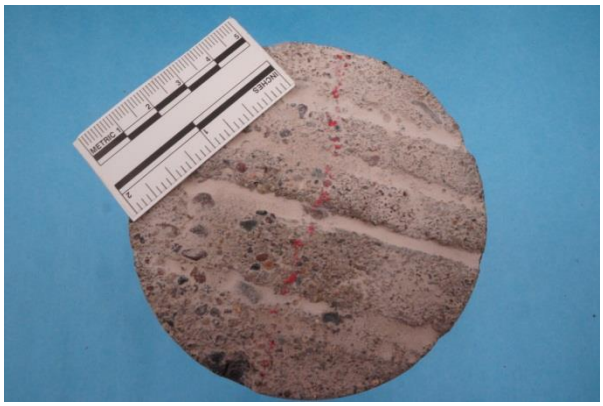

Figure 3. Photographs of Core 3.

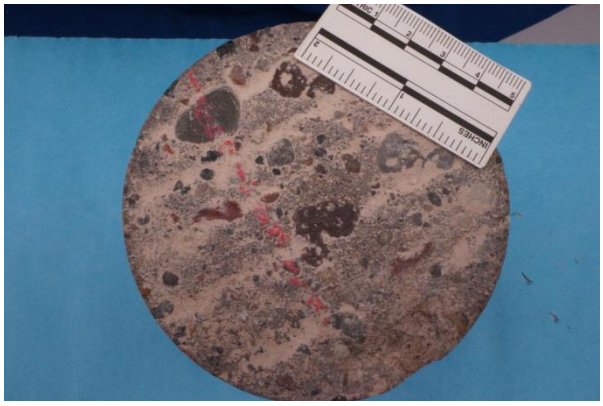

Figure 4. Photographs of Core 4.

Figure 5. Photographs of Core 5.

Figure 6. Photographs of Core 6.

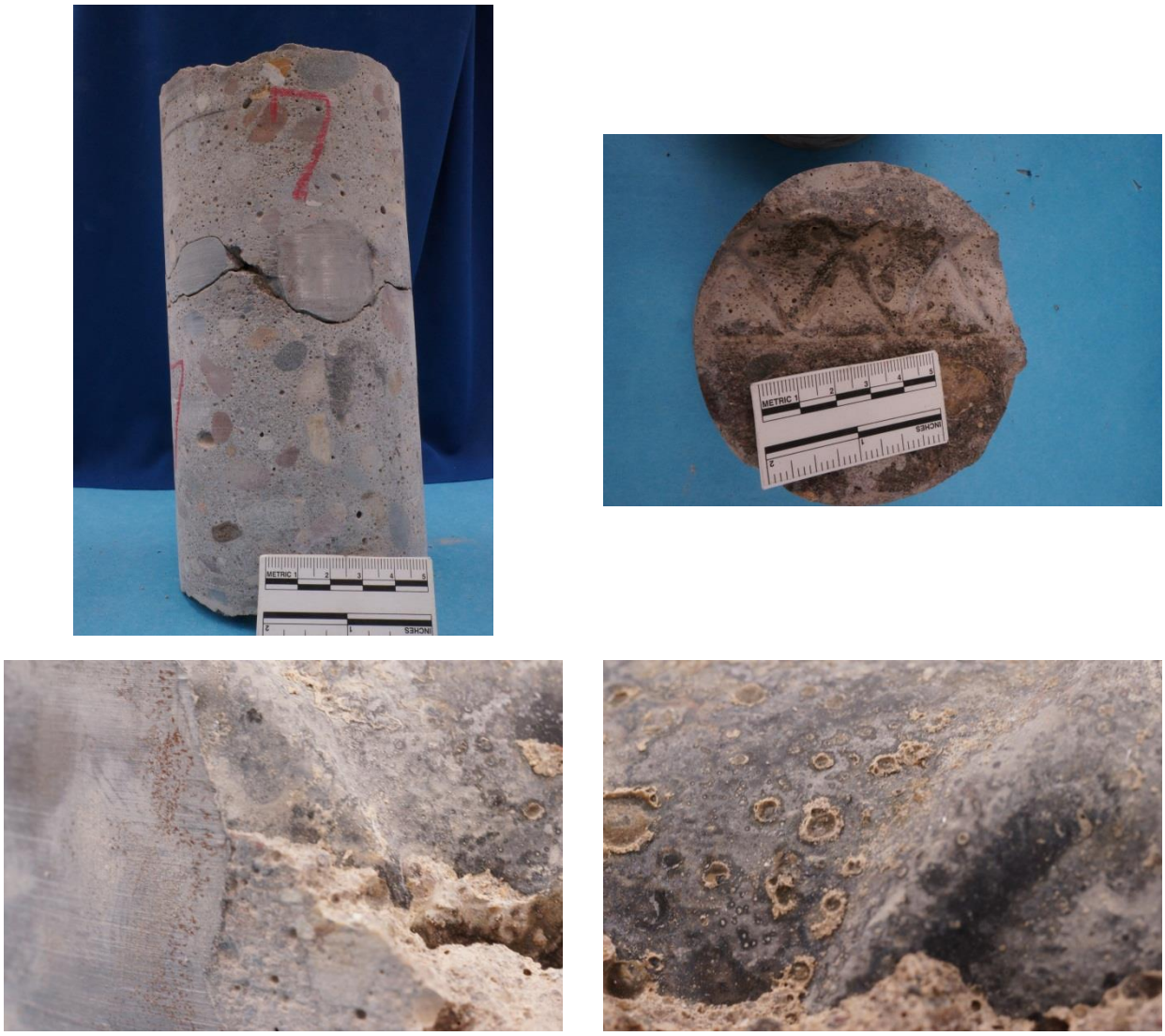

Figure 7. Photographs of Core 7.

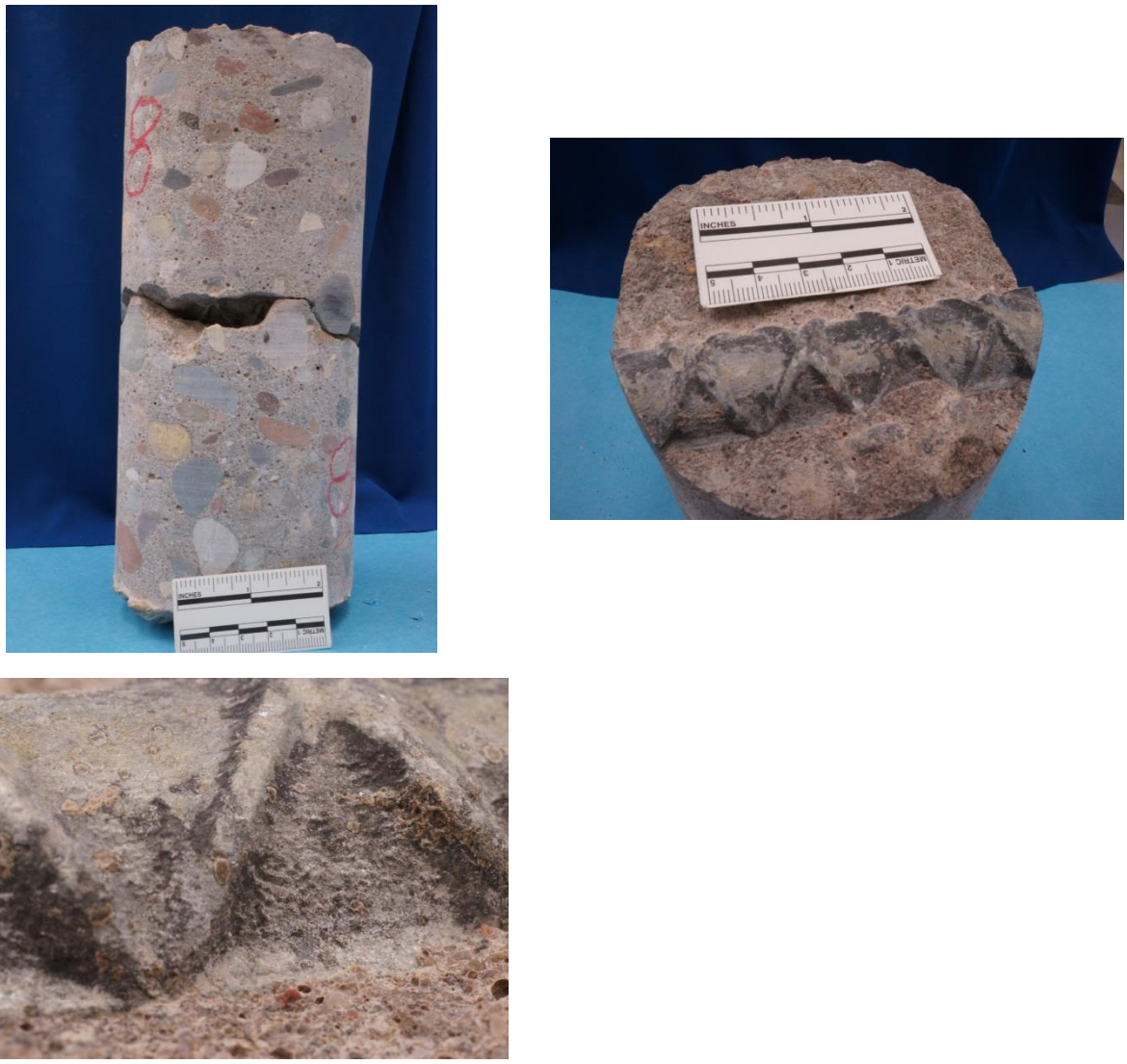

Figure 8. Photographs of Core 8.

Figure 9. Photographs of Core 9.

Figure 10. Photographs of Core 10.

WJE ENGINEERS ARCHITECTS MATERIALS SCIENTISTS

APPENDIX C

Petrographic Examination

WJE ENGINEERS ARCHITECTS MATERIALS SCIENTISTS

Wiss, Janney, Elstner Associates, Inc.
330 Pfingsten Road
Northbrook, Illinois 60062
847.272.7400 tel | 847.291.5189 fax
www.wje.com

INTEROFFICE MEMORANDUM

Via: Project Folder

To: Paul Krauss

From: Uznanski, Lidia L.

Date: February 22, 2013

Project: Iowa State Highway 92 Over Drainage Ditch #25
WJE No. 2012.5759

Subject: Concrete Petrography

PETROGRAPHIC STUDIES OF CONCRETE

Petrographic examination of concrete samples provides useful information on the concrete constituents and durability. Core 8 was examined petrographically using methods of ASTM C856, "*Standard Practice for Petrographic Examination of Hardened Concrete*." The examination was performed using stereoscopic and petrographic microscopes at magnifications ranging from 10x to 600x. Powder mounts were employed in the examination using the polarized-light microscope. The examined sections of the core include top 3-inch and the bottom 3-1/2-inch sections of the core. Horizontal slices had been removed from mid-depth of the core for chloride analyses prior to receiving the sample for petrographic studies.

Additionally, the top regions of six cores were tested for the depths of carbonation of the cement paste. The measured depths of carbonation are provided in Table 1. This testing could not be conducted on four other cores because the top sections of those cores were consumed in other testing.

Core 8

Condition - The top surface of the concrete exhibits rake marks. The top surface is slightly weathered and somewhat uneven. A few aggregate particles have been dislodged from the top surface of the concrete. The concrete mix appears uniform and well consolidated throughout the core sample. The lower section of the core contains an impression of a reinforcing bar. (Figure 1). Corrosion staining was not observed.

A few fine microcarcks were detected on the lapped surfaces of the sample (Figures 1, 2, and 3). One microcrack slopes at an angle from the top surface and exits from the side of the core at the depth of 3/4 inch. It splits into a few finer microcracks just below the top surface. The second main microcrack is found in the bottom section of the core. This microcrack extends from the cut, bottom surface mostly through the section, terminating approximately 1/4 inch below the top of that section. The microcrack appears slightly wider near the cut (bottom) surface than near the fractured/cracked (top) surface. Both microcracks mainly pass around aggregate particles. Impression of a rebar is visible in the middle section

of the core. The widths of the microcracks are 1 mil or less. The microcrack in the top region of the concrete may be shrinkage/carbonation-related, and the microcrack in the lower region of the core could also be related to shrinkage or it could be due to flexural stress.

Small amounts of secondary mineral deposits, mainly calcium hydroxide, some ettringite, and possibly deicing salts, were detected inside some air-voids only in the top ¼ inch of the concrete (Fig.4). This suggests that the concrete from this particular area is moderately dense or was not subjected to a lot of moisture.

Aggregate - Coarse aggregate represents siliceous and calcareous gravel having maximum nominal size of 3/4 inch. It is composed of variety of rock types that include granite, limestone, volcanic rocks, quartzite, sandstone, siltstone, chert, and small amounts of other rocks. Some of the sedimentary rocks, sandstone and siltstone, are somewhat soft and absorbent, but there is no indication of problems associated with those particles within the concrete. The chert particles occur in two forms; hard and dense, and somewhat soft and porous. Some of the chert particles exhibit reaction rims as observed on the lapped surfaces of the core. However, there is no indication of alkali-silica reaction (ASR); secondary deposits of silica gel were not detected. Fine aggregate is natural siliceous sand composed mainly of quartz and small amounts of igneous rocks. The aggregate is well graded and uniformly distributed within the concrete. The total aggregate content appears somewhat lower than in average concrete, resulting in slightly higher content of the cement paste estimated at 30 percent by volume. The aggregate particles are well bonded to the cement paste.

Paste - The cement paste is moderately hard to hard and moderately dense. The estimated cement content is 6 to 7 bags per cubic yard of concrete. The water cement ratio is overall relatively low, estimated to range from 0.38 to 0.45; some variability were detected on a micro-scale. Hydration of the cement is moderately advanced to advanced and normal. Pozzolans were not detected within the mix. The depth of carbonation of the cement paste ranges from 1/16 to 1/8 inch as measured from the top surface of the core.

Air - The concrete is air-entrained. The approximate air content is 6.5 to 7 percent. The air occurs mainly as small and medium size, spherical voids that are typical of entrained air, and a small number of medium size, irregularly shaped voids typical of entrapped air. The distribution of the air voids is generally uniform. The air voids are somewhat less frequent within the top 1/4 inch of the core.

Summary of Petrographic Studies

The petrographic examination of Core 8 indicates that the concrete mix contains siliceous and calcareous gravel coarse aggregate and natural siliceous sand fine aggregate. The cement paste is strong and of good quality. The estimated water-cement ratio is 0.38 to 0.45, and the approximate cement content is 6 to 7 bags per cubic yard of concrete. Pozzolans were not detected. The concrete is air entrained and contains 6.5 to 7 percent air. The air void system is of good quality and is judged to be adequate for proper protection of the concrete from possible cyclic freeze-thaw damage.

A few longitudinal microcracks were detected within the concrete. Two main microcracks included one in the top 3/4 inch of the core and one in the bottom 3 inches of the core. The microcracks are very fine with widths measuring 1 mil or less, and mainly pass around aggregate particles. These microcracks may be

related to shrinkage and flexing of the slab. The tiny microcracks branching off the main microcracks near the very top of the core most likely are related to carbonation shrinkage of the cement paste.

Small amounts of secondary mineral deposits were detected inside air voids along top surface of the concrete. The scarcity of the secondary deposits indicates that the concrete remained relatively dry or impermeable while in service. There was no evidence of ASR associated with chert particles present within the aggregate.

Storage: Thirty days after completion of our studies, the samples will be discarded unless the client submits a written request for their return. Shipping and handling fees will be assessed for any samples returned to the client. Any hazardous materials that may have been submitted for study will be returned to the client and shipping and handling fees will apply. The client may request that WJE retain samples in storage in our warehouse. In that case, a yearly storage fee will apply.

Table 1 - Depths of carbonation of the cement paste

Core ID	Depth of paste carbonation from exposed surface (inch)
1.	1/8 to 1/4
2.	1/16 to 1/8
3.	1/8 to 1-1/4 (carbonation might partially coincide with pre-existing microcrack)
7.	1/4
8.	1/16 to 1/8
10	1/8 to 1/4

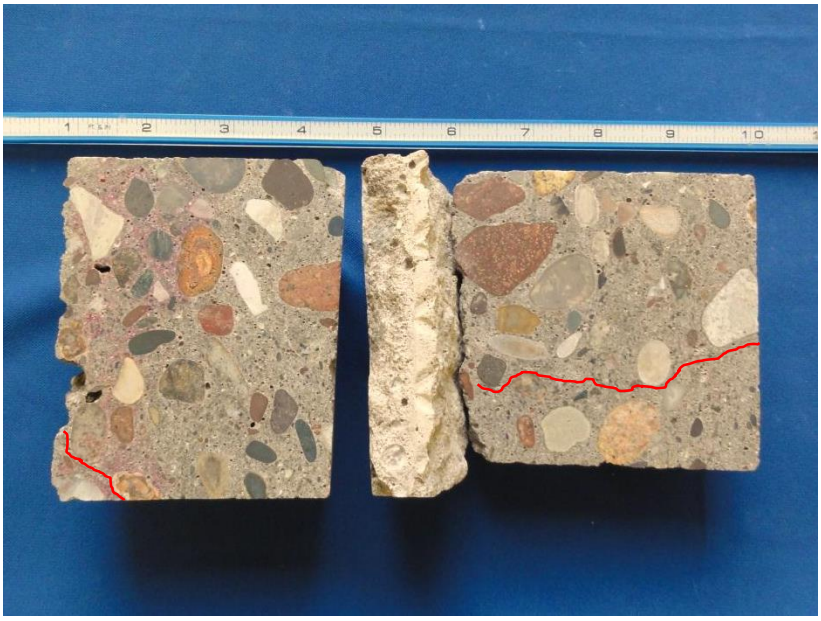

Figure 1. Sections of Core 8; top surface of the concrete is on the left of the photograph. The locations of the microcracks are outlined in red. Impression of a rebar is visible in the middle section of the core. Similar impression (not visible in photo) is also present at the top of the bottom section.

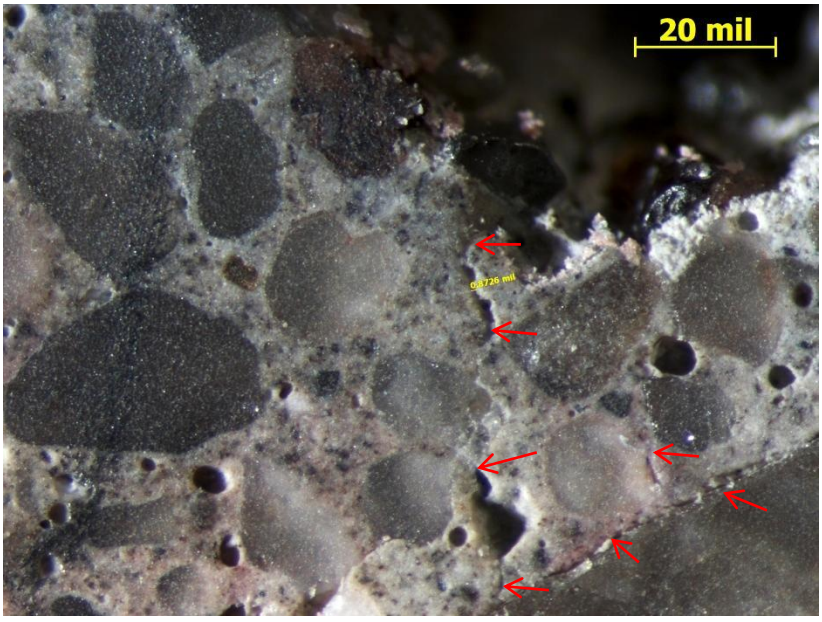

Figure 2. Lapped surface of Core 8 just below the top. The main microcrack split into a few tiny microcracks (indicated by red arrows) just below the very top surface of the core.

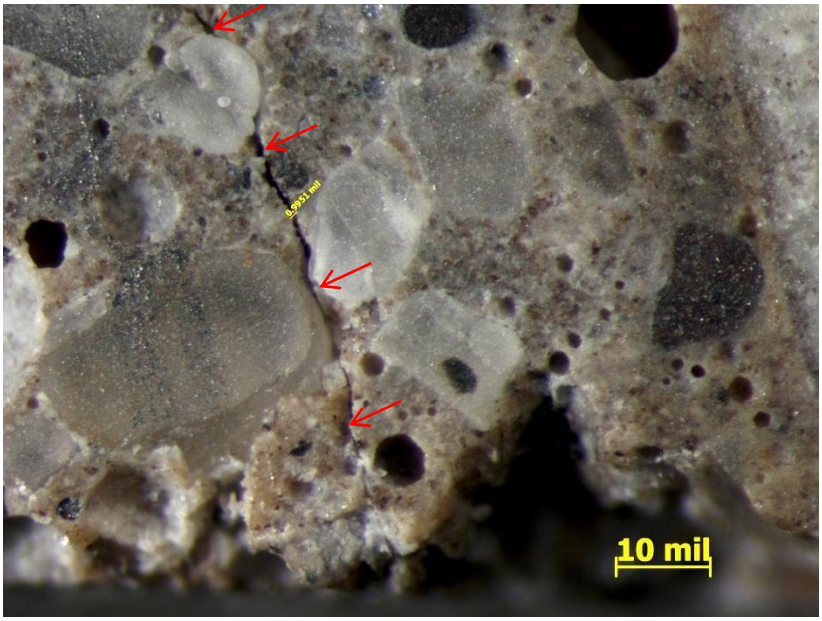

Figure 3. Shown is a microcrack (indicated by red arrows) on the lapped surface in bottom region of Core 8.

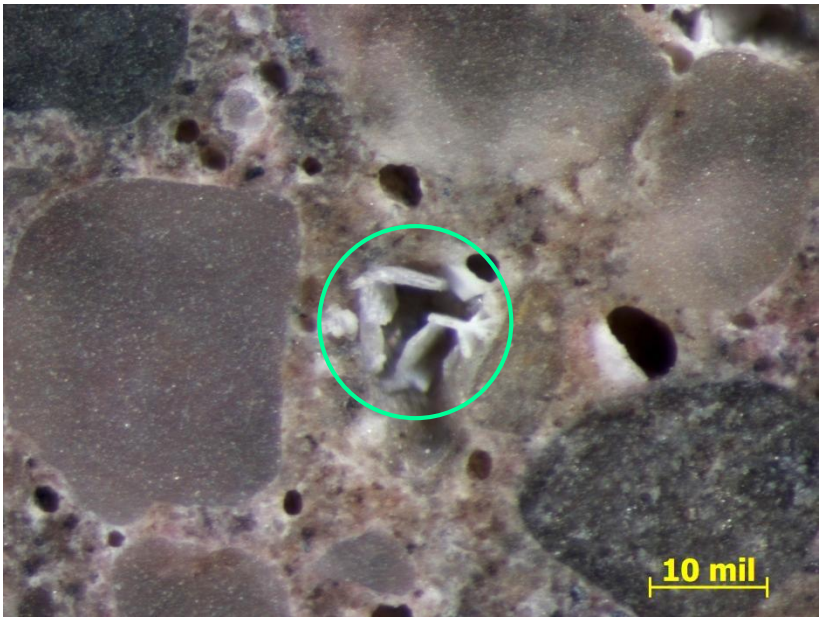

Figure 4. Lapped surface just below the top of Core 8 showing secondary deposits of calcium hydroxide inside an air void (encircled).

WJE ENGINEERS ARCHITECTS MATERIALS SCIENTISTS

APPENDIX D

Laboratory Analysis of Reinforcing Bars

LABORATORY EXAMINATION OF REINFORCING BAR SAMPLES

Galvanized reinforcing bars were removed from concrete cores taken from the topside of the bridge deck. Excess concrete was removed from the bars where possible. Selected bars were examined to evaluate the corrosion product, the degree of pitting, and the thickness of the zinc layer. The bar samples were selected to encompass a range of chloride levels within the concrete. Sample 8 had a very low level of chloride at the bar (0.004 percent by mass). Samples 3 and 7 had slightly higher levels of chloride at the level of the bar (0.050 and 0.084 percent by mass, respectively). Samples 9 and 10 had significantly higher levels of chloride at the level of the bar (0.193 and 0.376 percent by mass, respectively).

Evaluation of the Corrosion Product

The corrosion product on the exterior of the bar samples was evaluated visually using a stereomicroscope, and two specimens were further analyzed to determine composition.

Visual and Microscopical Evaluation

Sample 8 (low chloride level)
The bottom surface of Sample 8 has areas of both light green-gray shiny surface and dark gray surface. White deposits are present in limited areas. The top surface of the bar is uniform dark gray indicating the absence of corrosion. Light white discoloration may indicate minor surface corrosion of the bottom side of the bar. Photographs and micrographs of the sample are provided in Figure 1 through Figure 3.

Sample 3 (moderate chloride level)
The surface of Sample 3, where not covered with adherent concrete, was light gray, shiny with a metallic appearance on the bottom of the bar. White deposits were present in one area of the bottom of the bar indicative of zinc surface corrosion. The top of the bar had a darker gray appearance with the absence of notable corrosion. Photographs and micrographs of the sample are provided in Figure 4 through Figure 7.

Sample 7 (moderate chloride level)
The bottom surface of Sample 7 was lighter in color than the top surface. The appearance ranged from light gray to slightly green and shiny, to spots of white deposit, and a few spots of yellow-green deposit. Surface corrosion of the zinc is likely along the bottom surface of the bar. The top surface had more adherent concrete, but where the bar was exposed, was a uniform dark gray and corrosion was absent. Photographs and micrographs of the sample are provided in Figure 8 through Figure 12.

Sample 9 (high chloride level)
The bottom surface of Sample 9 is covered primarily in white corrosion deposits, although some localized areas have no apparent deposit. The top surface is primarily red corrosion product, with some white corrosion product present. This indicates that the zinc layer has been mostly consumed. Photographs and micrographs of the sample are provided in Figure 13 through Figure 15.

Sample 10 (high chloride level)
The bottom surface of Sample 10 consists primarily of white and red corrosion product, with some gray surface visible. The top surface consists primarily of red corrosion product, with a stripe of blue-gray deposit near the side of the bar. Corrosion is wide spread and the zinc has been consumed in areas. Photographs and micrographs of the sample are provided in Figure 16 through Figure 20.

Compositional Analysis of Corrosion Product

Compositional analysis of Sample 8 (low chloride) and Sample 10 (high chloride) was performed using scanning electron microscopy with energy dispersive x-ray spectroscopy (SEM/EDS). The corrosion products of Sample 10 were further analyzed using x-ray diffraction (XRD).

In SEM, a beam of electrons is generated, focused, and scanned across a very small area of the sample. The electrons interact with the sample in many ways, which can be used to image and analyze the sample. Two imaging modes are possible: backscattered and secondary. During backscattered electron (BE) imaging, the electron beam bombards the sample, and some electrons are backscattered or elastically scattered by the elements in the sample based on their atomic number. Heavier atoms in the sample scatter the beam electrons more than lighter atoms; hence phases with a higher average atomic weight appear brighter in the resulting image than phases with a lower average atomic weight, providing compositional information within the image. Secondary electron (SE) imaging uses electrons that are emitted from the sample as a result of inelastic interactions with the beam. SE images provide information related to the topography of the specimen; cracks and crystals deposited on the surface will be well defined. The interaction of beam electrons with the sample also generates characteristic x-rays. The energy of the characteristic x-rays can be measured using an EDS, and the elements present in the sample can be identified. EDS can only identify elements heavier than boron (carbon through uranium); therefore lighter elements, such as hydrogen, do not appear in the spectrum. EDS data can be collected from a point a few microns across, or over a larger area of the sample. Prior to analysis by SEM/EDS a sample is typically coated by a thin layer of conductive carbon. This carbon is apparent in the EDS spectrum. Therefore, for some samples, it cannot be determined if the carbon is from the sample itself or the carbon coating.

In addition to imaging and EDS spectra, the SEM can generate a dot map. In x-ray dot mapping mode the localized distributions of selected elements are shown in separate boxes. Each box is labeled to identify the element being represented in that box. The presence of an element in an area on the sample is indicated by a concentration of dots.

XRD analysis is suitable for identifying crystalline compounds; non-crystalline compounds do not have a definite XRD pattern. During x-ray diffraction analysis, radiation produced from an x-ray source is diffracted off the sample at various angles. A detector measures the intensity of the diffracted energy, and the location (angle) and intensity are recorded as a graph. This graph, which displays a pattern of peaks, can be interpreted to identify the crystalline components of the sample. The peaks are compared to a library of diffraction patterns of known components.

Sample 8 (low chloride level)

Sample 8 had a distinct dual-color appearance, with the top of the bar (as it was placed in the slab) having a dark gray appearance, with a lighter gray/silver/white appearance on the bottom of the bar (Figure 21). To evaluate compositional differences between the two colors, the surface of Sample 8 was examined using SEM/EDS.

No significant compositional differences were observed between the darker and lighter portions of the bar (Figure 22 and Figure 23). Both consist primarily of zinc and oxygen, with varying amounts of calcium, and small quantities of aluminum, silicon, sulfur, lead, chromium, and iron. The zinc is from the

galvanizing layer, the oxygen is present either as some oxidation of the zinc or from residual cement paste adhered to the bar. The calcium, aluminum, silicon, and sulfur are present from residual cement paste. The lead is present as an impurity in the zinc. The iron and chromium may be present from the bar itself.

Sample 10 (high chloride level)

A cross-section of Sample 10 was examined using SEM/EDS to evaluate the composition of the corrosion product and zinc layer. A large pit filled with iron corrosion product was examined. Significant, but varying, amounts of chlorine were detected in different layers of the corrosion product (Figure 24). This confirms a chloride-induced pitting mechanism. Examination of the zinc layer indicated corrosion (oxidation) beginning at the exterior (Figure 25). Little to no chlorine (beyond the small amount present in the epoxy mounting medium) is present in the zinc layer that is beginning to corrode.

A small amount of concrete remained adhered to the rebar of Sample 10 in the location prepared for cross-sectional analysis. This portion was examined in detail to determine if the corrosion product diffused into the concrete. Dot map analysis indicated that iron and zinc corrosion product penetrated through cracks in the concrete, but do not appear to have diffused into the concrete itself (Figure 26). It is not known if the cracks existed prior to the corrosion of the reinforcing bar.

White corrosion product (from corrosion of the zinc layer) was removed from Sample 10 for analysis using XRD. XRD detects crystalline components of a material. Unlike SEM/EDS, which provides elemental composition, XRD provides the ways in which the elements are combined. However, not all corrosion products are crystalline, so XRD does not provide a complete picture of all compositions present, and typically is used in conjunction with SEM/EDS. XRD analysis of white corrosion product from Sample 10 indicated the presence of zincite (ZnO) and zinc hydroxide [$Zn(OH)_2$], both common corrosion products of zinc.

Coating Thickness Measurements

Sections of bars from Cores 3, 7, 8, 9, and 10 were examined to determine the presence and thickness of zinc coating. The bars were cut in cross-section, embedded in a thermoset resin, and polished to produce a surface suitable for microscopy. To measure the thickness of the zinc layer, the cross-sections were examined using a reflected light microscope. Measurements were made using a calibrated scale reticle in the eyepiece. Twelve measurements were collected on Sample 8 and 4 (3/4 inch diameter, #6 bars), while twenty measurements each were collected on Samples 7, 9 and 10 (1-1/4 inch diameter, #10 bars). Results are presented in Table 1. Measurements of 0.0 mils indicate that no zinc layer was present at that location.

The thickness measurements indicated that metallic zinc is present in areas while completely corroded through in others. Samples 9 and 10 both exhibited surface corrosion, including white corrosion (zinc) and red corrosion (steel) and came from cores with significant chloride concentrations at the bar level. Pitting and significant zinc loss was also observed on Samples 9 and 10. The greatest degree of pitting was observed on the top surfaces (as placed in the slab) on both Samples 9 and 10. In contrast, little corrosion product was observed on Samples 3, 7, or 8. No difference in zinc layer thickness or degree of corrosion was apparent around the circumference of the bar; the thickness of zinc was the same on the top and bottom of the bar. Most of the zinc was consumed in Sample 9 and Sample 10 and pitting corrosion of the mild steel was noted. Micrographs showing the general condition of the zinc layers on the bar samples are provided in Figure 27 through Figure 35.

Table 1. Zinc Coating Thickness Measurements.

Reading	Zinc Coating Thickness (mils)				
	Sample 8	**Sample 3**	**Sample 7**	**Sample 9**	**Sample 10**
1	4.8	3.7	5.0	4.5	2.6
2	3.9	4.2	6.4	2.2	1.6
3	7.5	4.2	8.7	0.0	0.0
4	4.1	3.4	3.1	0.0	0.0
5	3.5	5.1	9.0	0.0	0.0
6	5.7	6.1	8.4	0.0	0.0
7	3.0	4.1	6.1	2.3	0.0
8	3.5	3.3	4.2	0.0	7.0
9	4.1	2.2	7.0	0.0	3.0
10	4.1	3.7	6.7	0.0	6.7
11	4.9	5.2	6.9	0.0	8.7
12	6.1	3.8	6.5	0.0	4.2
13			7.8	0.0	5.4
14			8.0	0.0	6.3
15			6.9	0.0	2.9
16			5.5	2.7	4.0
17			5.6	2.4	0.3
18			4.4	1.9	6.6
19			7.5	0.0	5.9
20			8.9	4.3	0.0
Minimum	3.0	2.2	3.1	0.0	0.0
Maximum	7.5	6.1	9.0	4.5	8.7
Average	4.6	4.1	6.6	1.0	3.3
Chloride content at bar level	0.004	0.050	0.084	0.193	0.376

Conclusions

The bars are hot-dipped galvanized and the zinc coating looks typical for this type of galvanizing. The zinc coating thickness in the samples exposed to 0.084 percent by mass of chloride were nominally similar and averaged between 4.1 and 6.6 mils, with individual measurements ranging from 2.2 to 9.0 mils. In this range of chloride concentrations, the zinc coating thickness of the bars did not appear to be affected by chloride, and it appears that these values are representative of the original coating thickness.

Samples 3, 7, and 8 were in chloride concentrations less than 0.084 percent and had intact zinc layers at every location measured around the circumference of the bar. They did contain limited white corrosion product present on the surface, most often on the underside of the bar. This underside corrosion may be due to incomplete contact with the concrete due to the minor settlement of the concrete away from the bottom of the bars or due to the trapping of bleed water beneath the bars. It is not uncommon for concrete settlement and bleed to alter the contact area of the bottom sides of reinforcing bars supported on chairs.

Significant loss of zinc thickness and underlying steel corrosion was observed in the two samples with chloride concentration greater than 0.193 percent by mass of chloride. Samples 9 and 10, from heavily chloride contaminated concrete, had intact zinc layers present only intermittently on the surface, and had pitting and red rust present on the surface. Sample 10, which had the highest chloride level, had the greatest amount of pitting present along the circumference studied.

The surface composition of Sample 8, chosen to represent a bar in non-chloride-contaminated concrete, consisted primarily of zinc, with some oxygen, and elements from the concrete that remained adhered to the surface. Although minimal oxidation of the surface was apparent from SEM/EDS analysis, the vast majority of the zinc layer was uncorroded.

Analysis of Sample 10, chosen to represent a corroded bar in chloride contaminated concrete, indicated the presence of chloride-induced corrosion in the pits, but little chlorine present in the intact or lightly corroding zinc layer.

Kimberly A. Steiner

Figures

Figure 1. Sample 8. Top side (left) and bottom side (right).

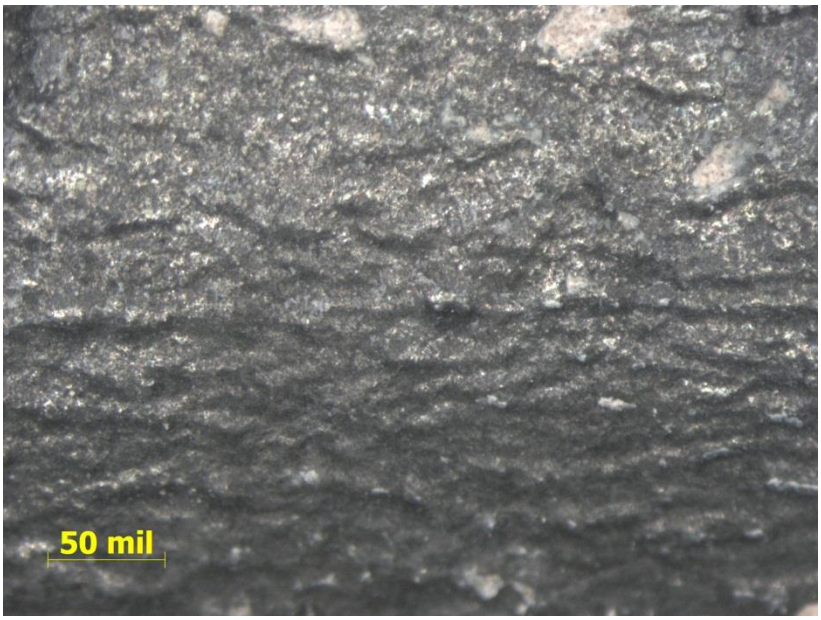

Figure 2. Micrograph of the top side of Sample 8. Note the uniform dark surface.

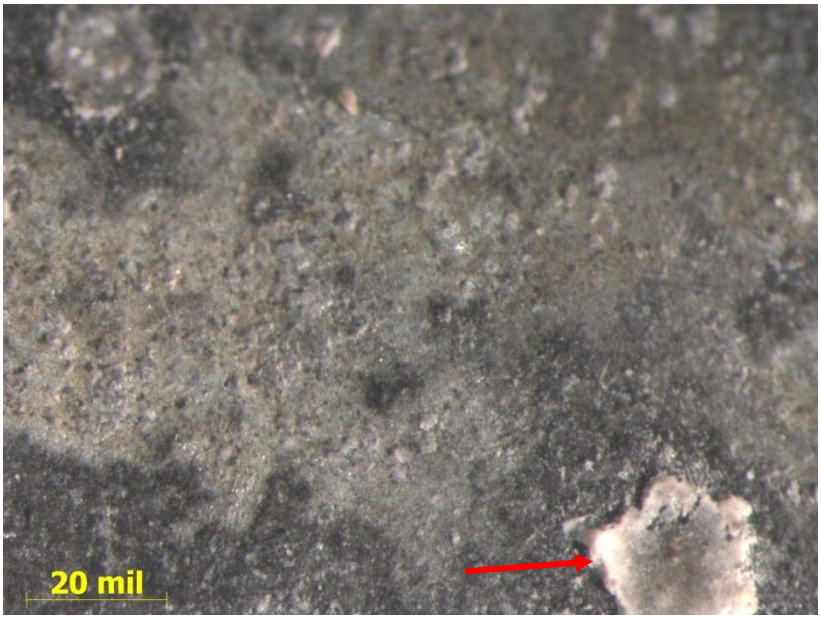

Figure 3. Micrograph of the bottom side of Sample 8. Note the dark to light coloration, with some white deposit indicated with an arrow.

Figure 4. Sample 3. Top side (left) and bottom side (right).

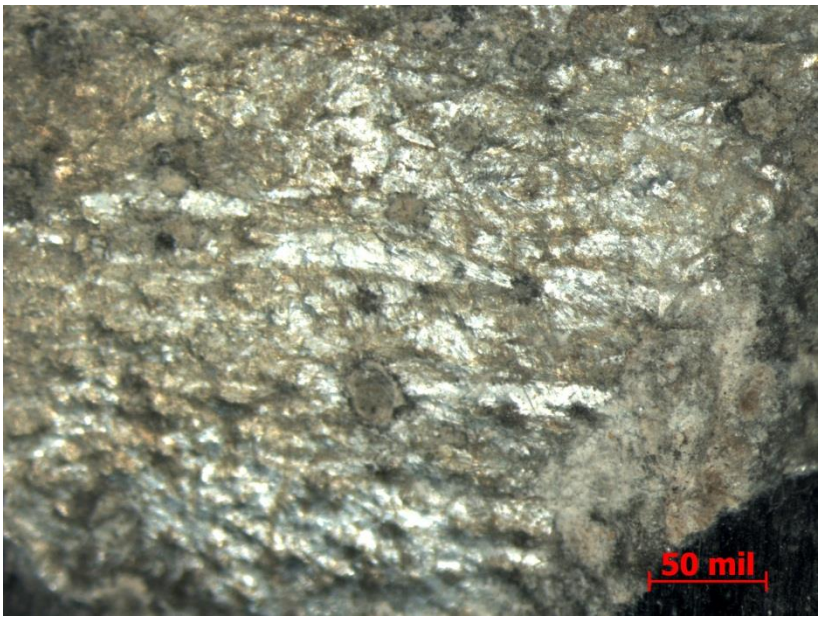

Figure 5. Micrograph of the bottom of Sample 3, showing the gray shiny surface.

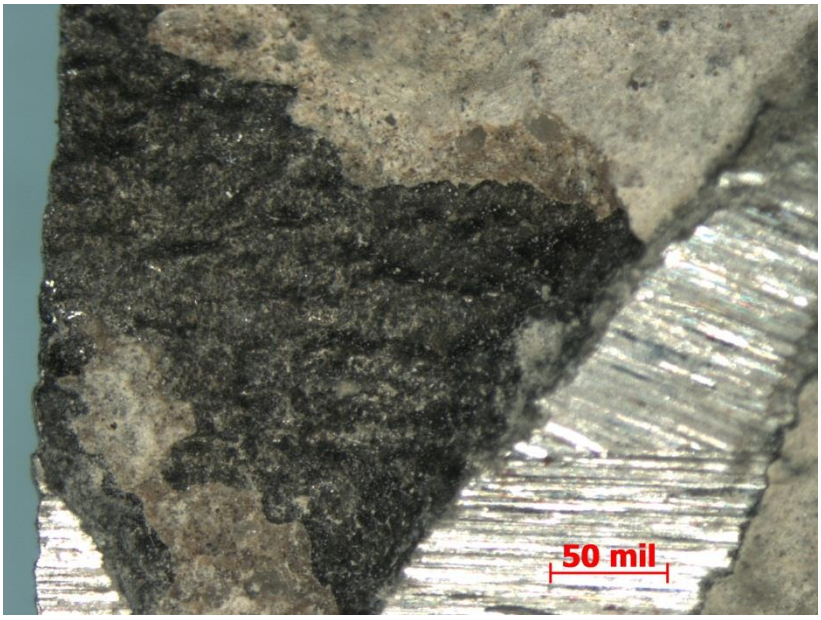

Figure 6. Micrograph of the top surface of Sample 3, showing the gray surface. The lighter color material on the surface is residual concrete.

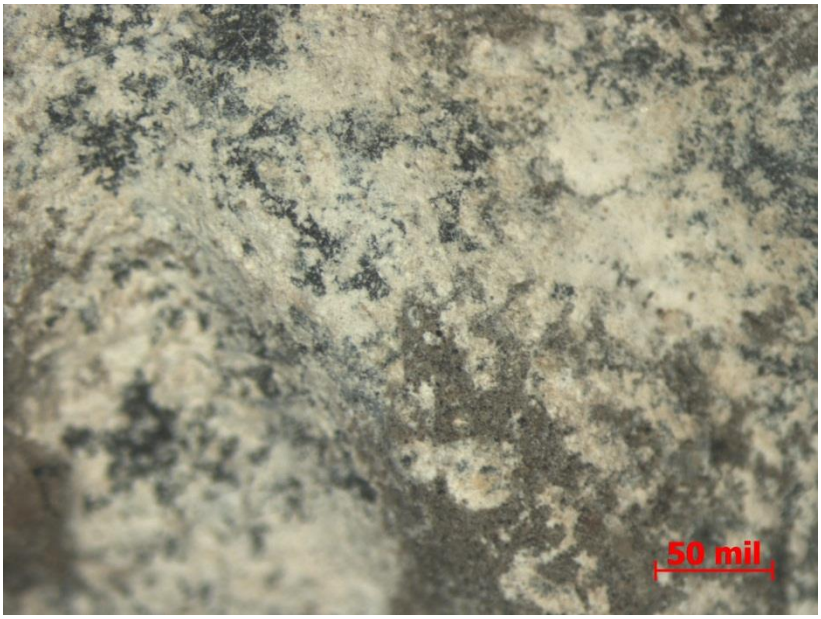

Figure 7. Micrograph of the top surface of Sample 3, showing white deposits.

Figure 8. Sample 7. Top side (left) and bottom side (right).

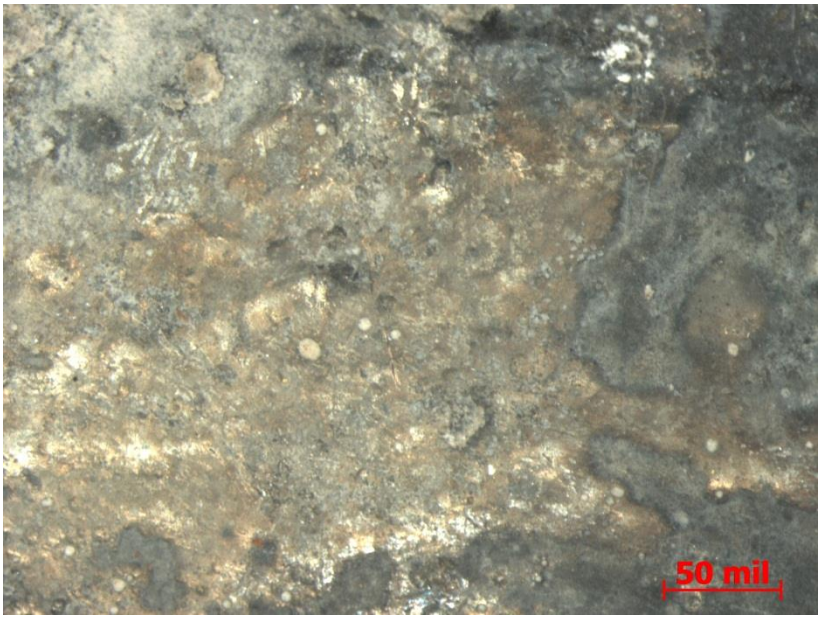

Figure 9. Micrograph showing the light green-gray shiny surface on the bottom of Sample 7.

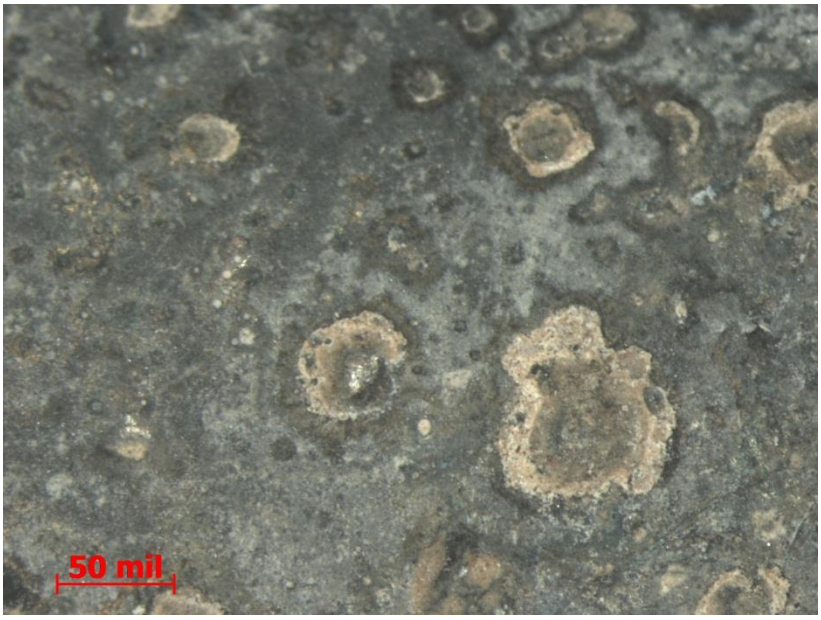

Figure 10. Micrograph showing the light gray surface of the bottom of Sample 7. The lighter colored deposits are adhered concrete.

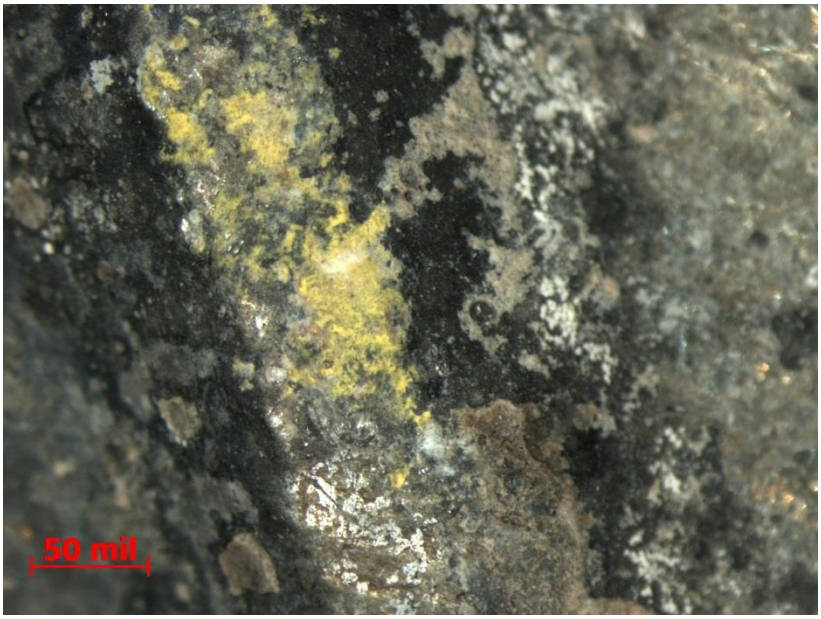

Figure 11. Micrograph sowing the yellow-green and white deposits on the bottom of Sample 7.

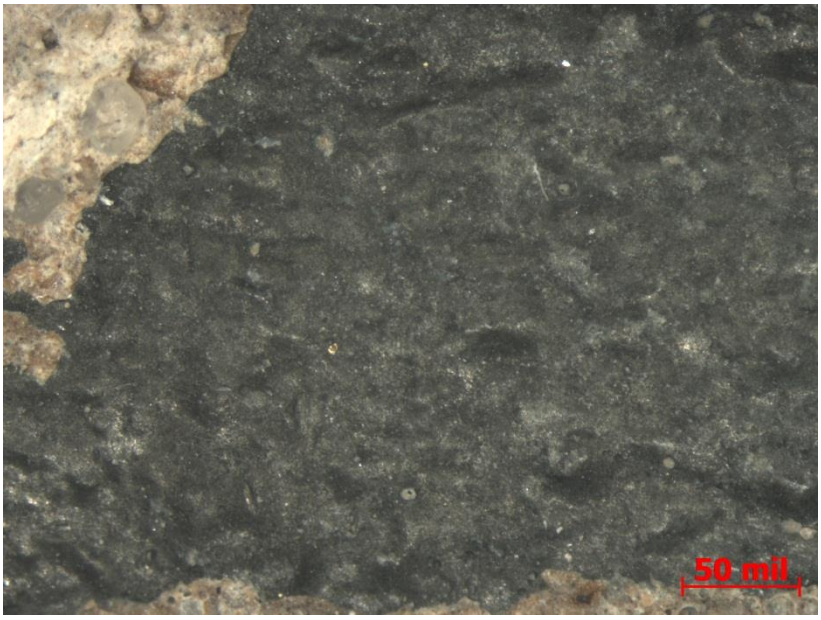

Figure 12. Micrograph showing the uniform, dark surface of Sample 7.

Figure 13. Sample 9. Top side (left) and bottom side (right).

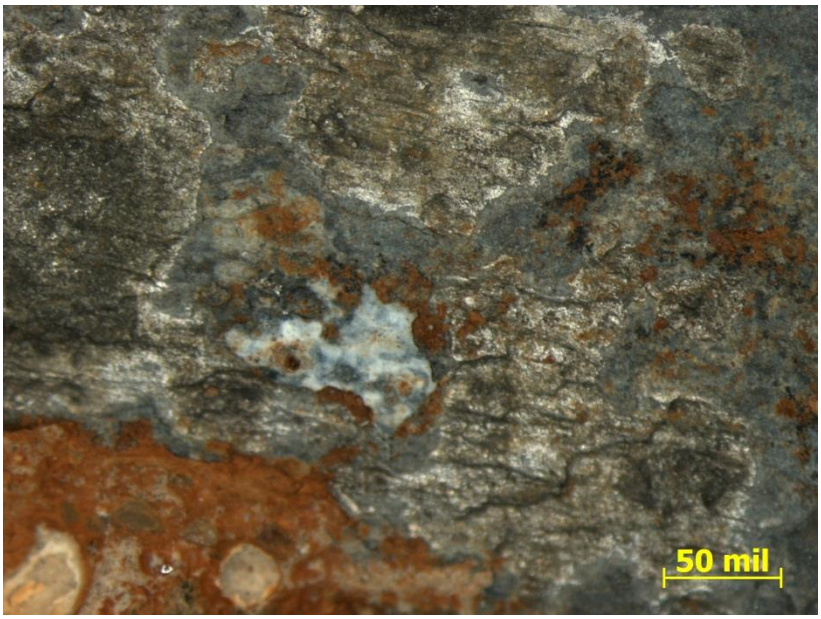

Figure 14. Micrograph of the bottom surface of Sample 9, showing localized areas with no deposits, nearby areas of white and red deposits.

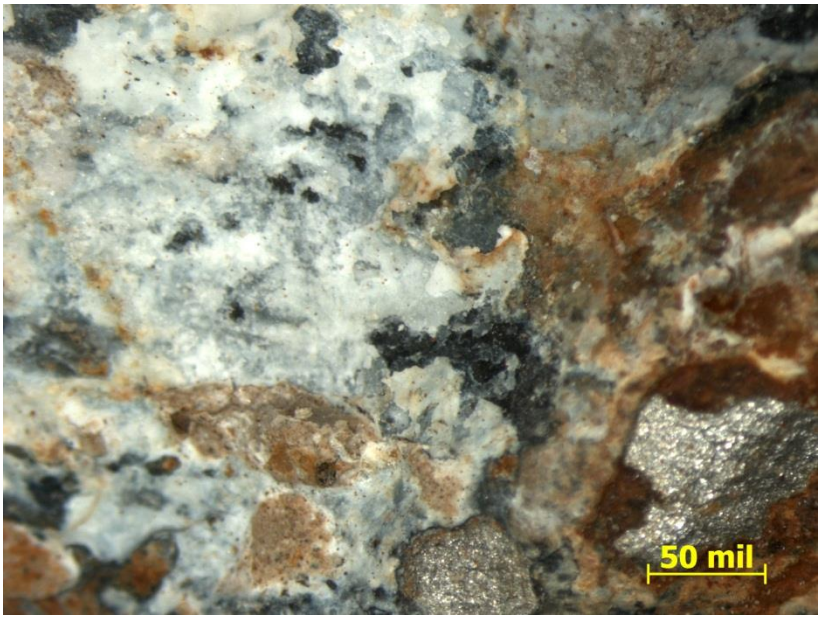

Figure 15. Micrograph of the bottom surface of Sample 9, showing white corrosion product.

Figure 16. Sample 10. Top side (left) and bottom side (right).The stripe of blue-gray deposit is indicated with an arrow.

Figure 17. Micrograph of the top surface of Sample 10, showing red corrosion product from the steel.

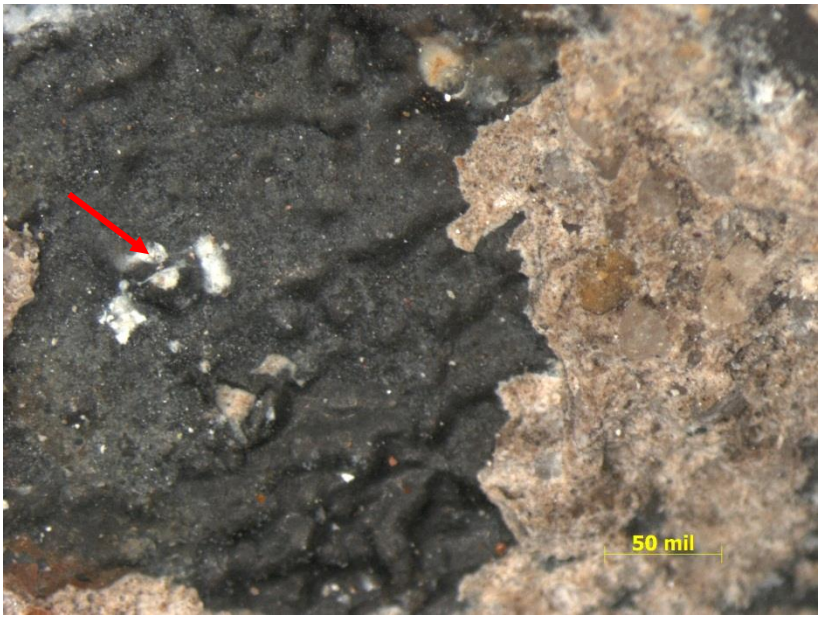

Figure 18. Micrograph of the side of Sample 10, showing concrete (indicated with an arrow) and a dark gray surface with only a small amount of white corrosion product.

Figure 19. Micrograph of the bottom surface of Sample 10, showing a white deposit.

Figure 20. Micrograph of the blue-gray deposit on the side of Sample 10.

Figure 21. Photograph of Sample 8, showing the dual colors. An arrow indicates which side faced up in the slab.

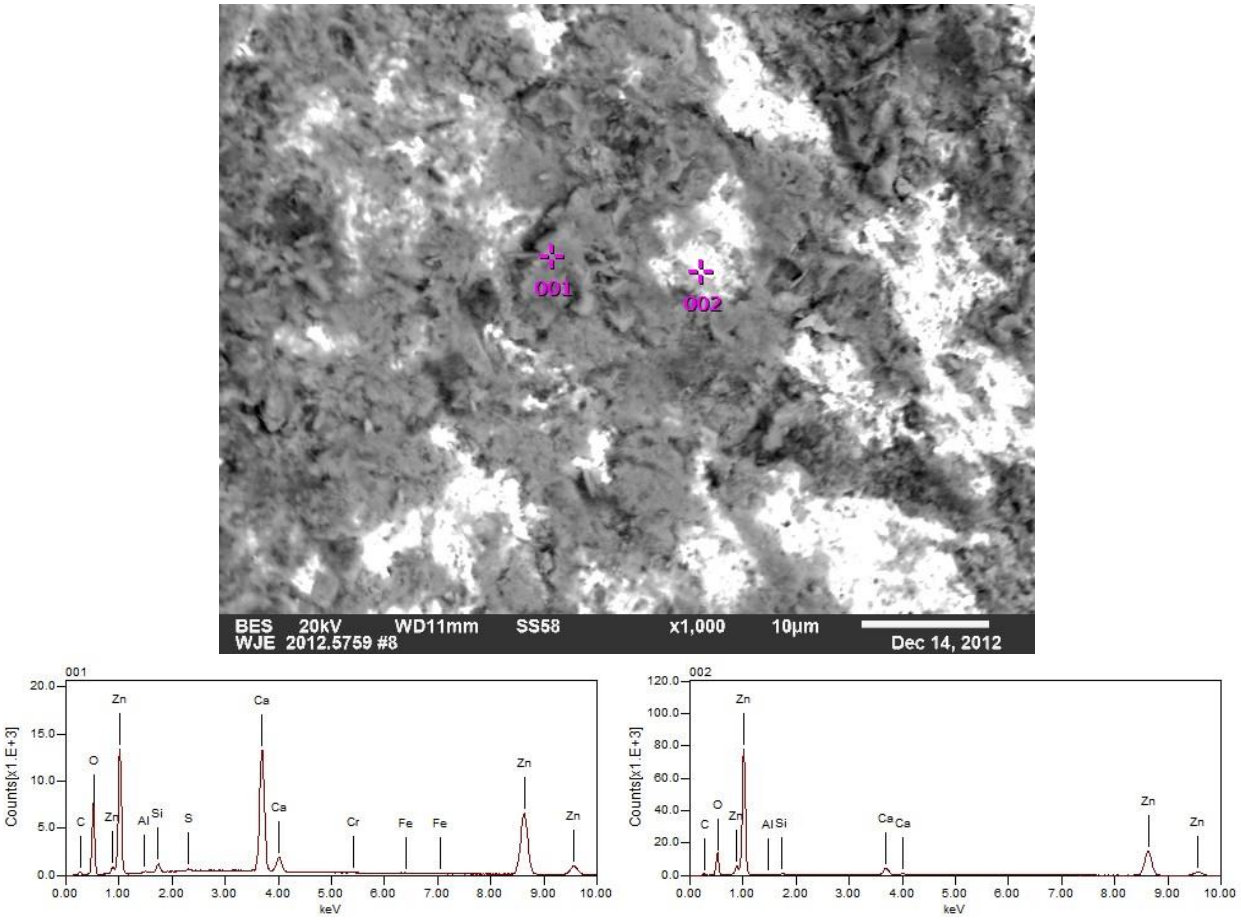

Figure 22. BE micrograph and point EDS spectra from the dark portion (top) of Sample 8. Each EDS spectrum has a number above the upper left corner which corresponds to the location indicated on the micrograph.

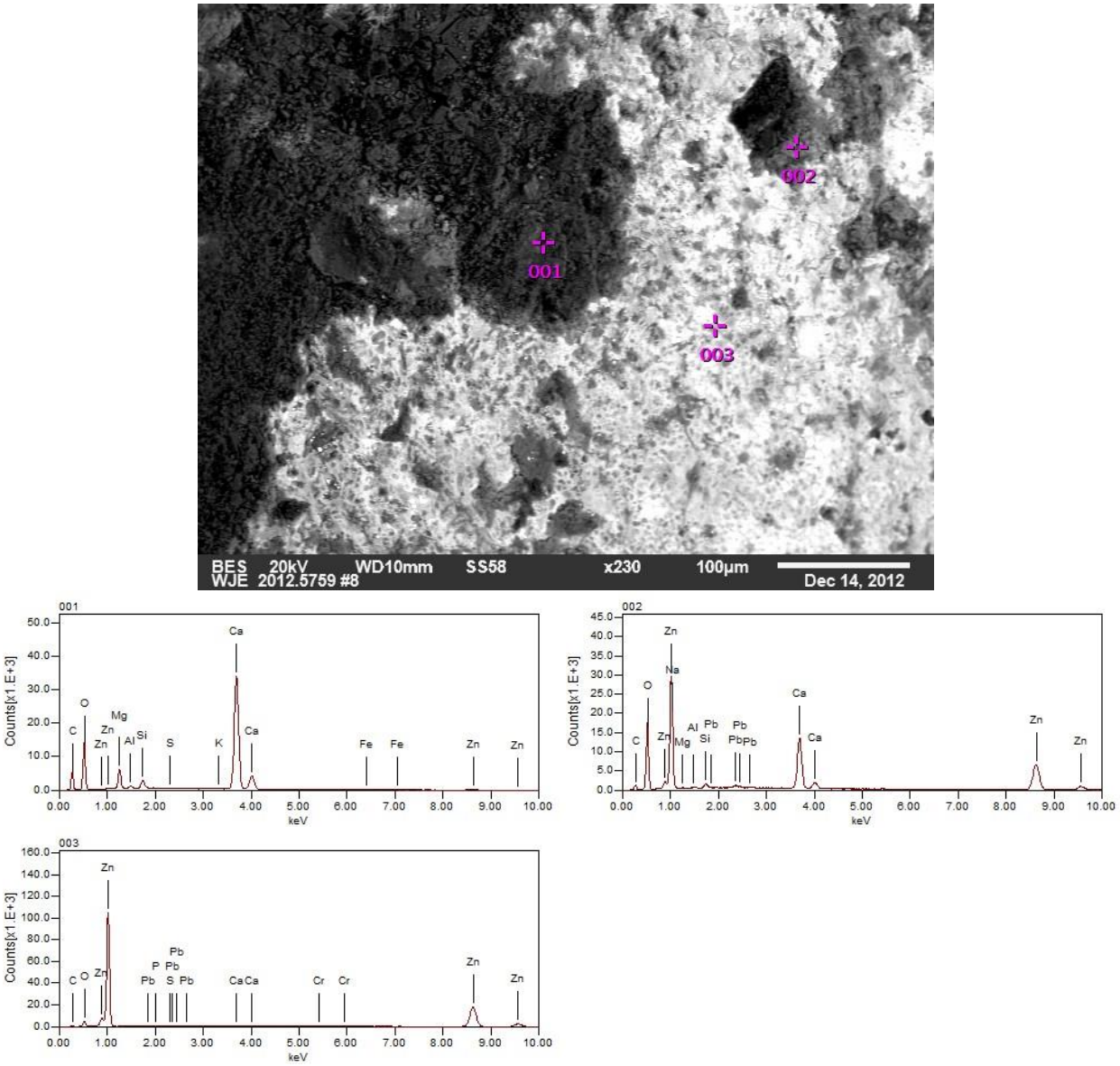

Figure 23. BE micrograph and point EDS spectra from the light portion (bottom) of Sample 8. Each EDS spectrum has a number above the upper left corner which corresponds to the location indicated on the micrograph.

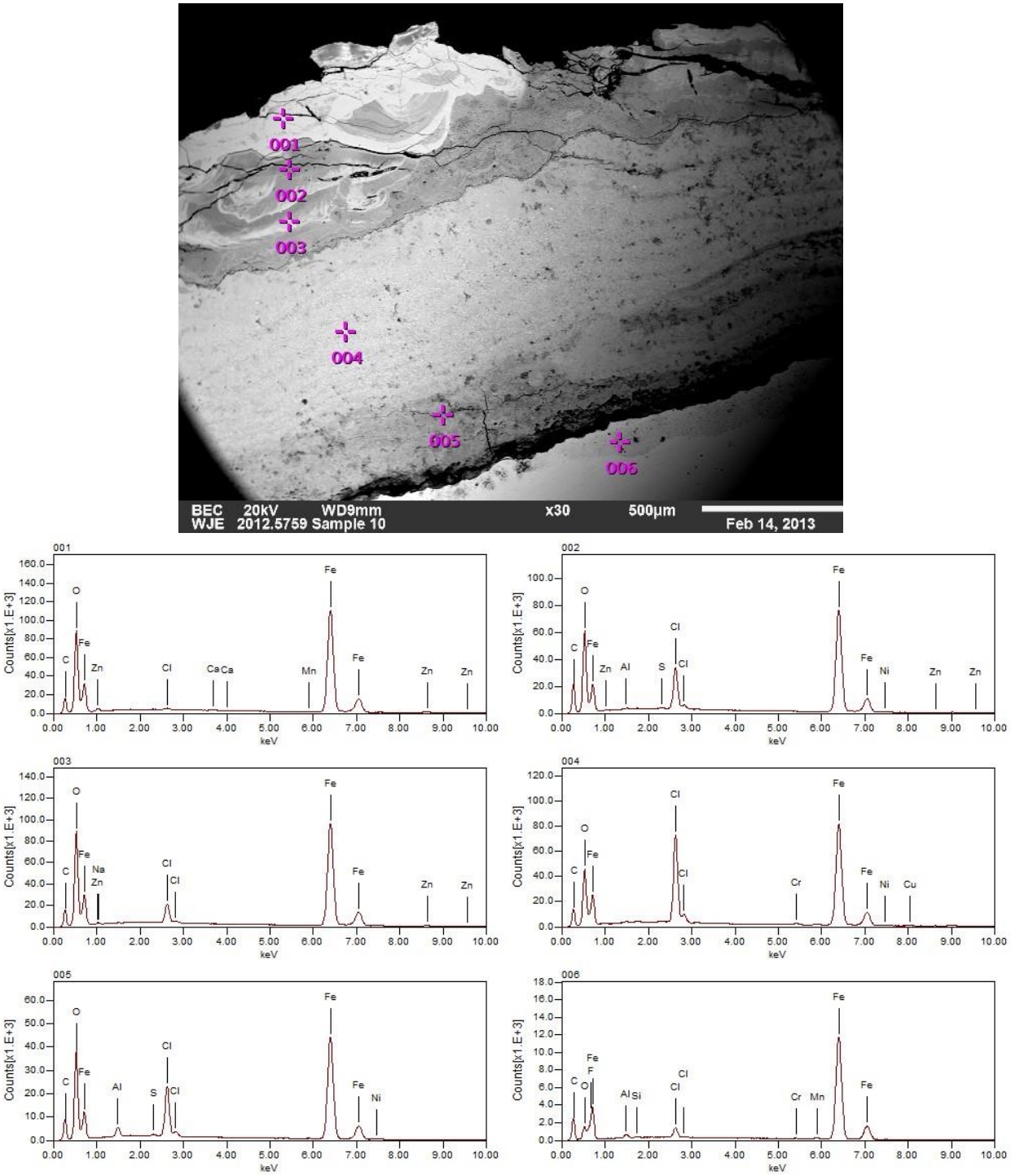

Figure 24. Cross-sectional BE image and point EDS spectra of a corroded pit on Sample 10, showing a significant amount of chlorine in the corrosion product. Each EDS spectrum has a number above the upper left corner which corresponds to the location indicated on the micrograph.

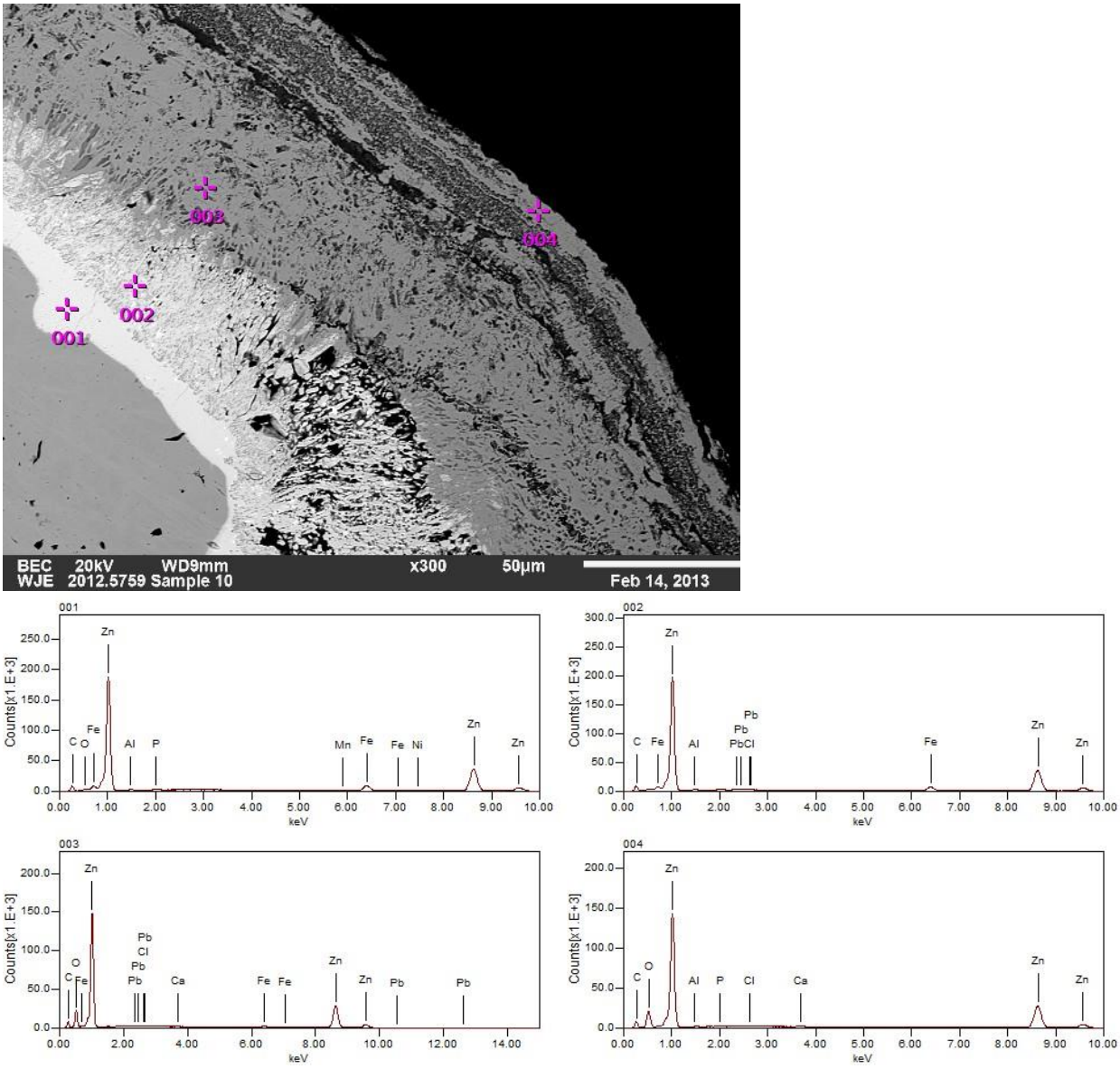

Figure 25. Cross-sectional BE image and point EDS spectra of the zinc layer Sample 10. Very little chlorine is incorporated into the zinc corrosion product (see EDS 004). Each EDS spectrum has a number above the upper left corner which corresponds to the location indicated on the micrograph. A minor amount of chlorine is present in the epoxy mounting medium.

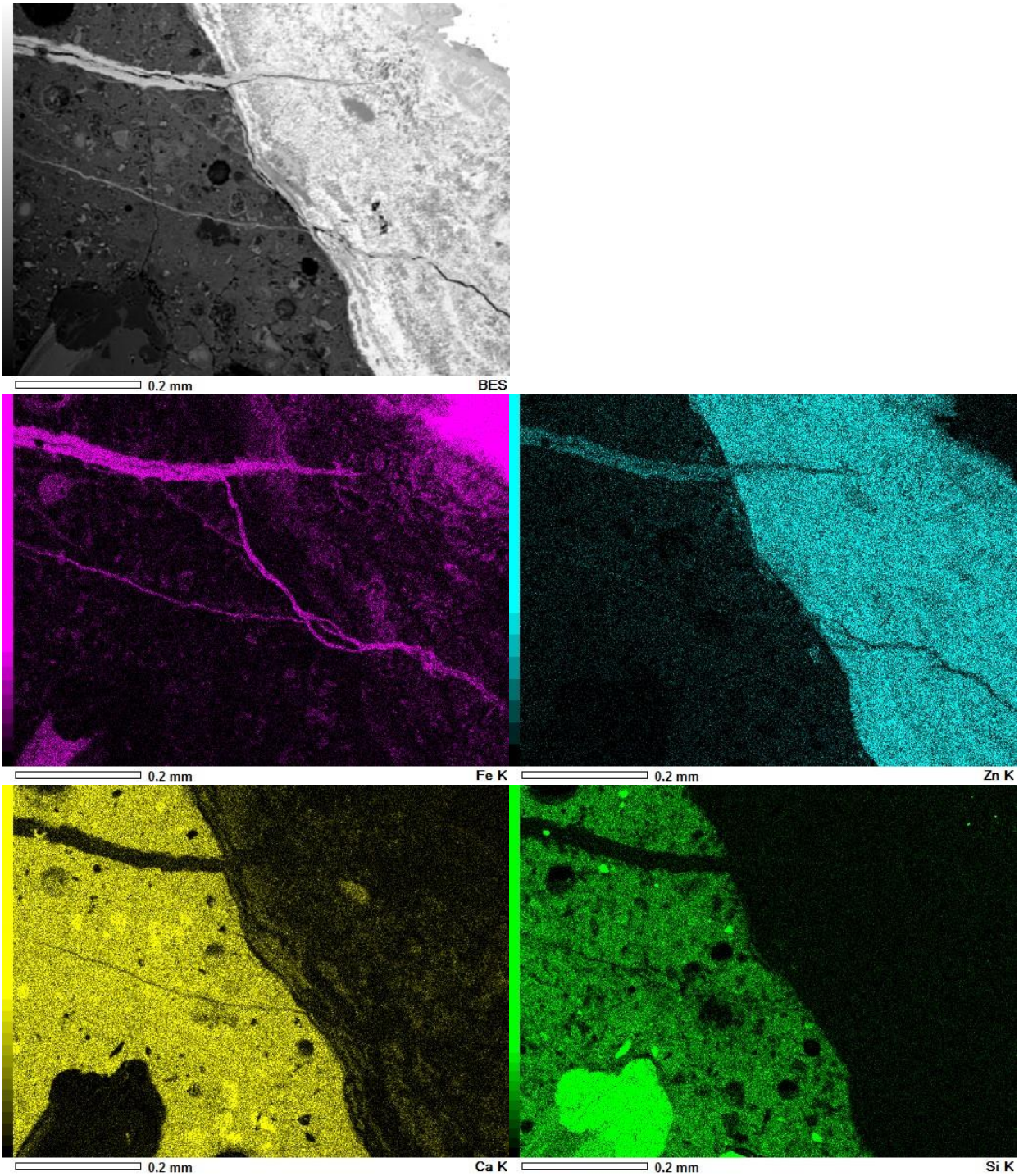

Figure 26. Dot map showing corrosion product/concrete interface of Sample 10. The corrosion product is on the right. The upper image is a BE micrograph. The elemental dot maps are, from left to right: purple -- iron, blue -- zinc, yellow -- calcium, green -- silicon. The iron and zinc can be seen penetrating the concrete along cracks, where calcium and silicon (constituents of cement paste) are not present.

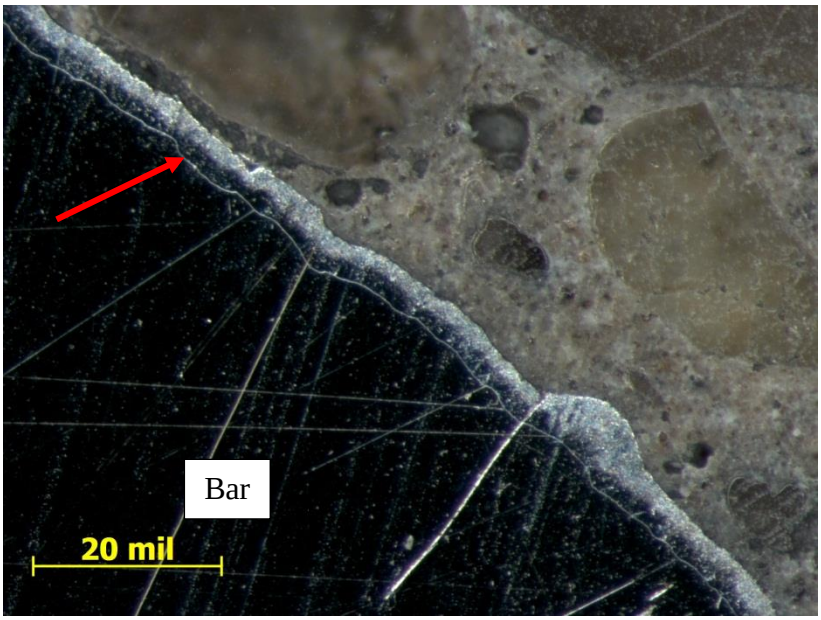

Figure 27. Cross-section of Sample 3, showing the bar, the zinc layer (arrow), and concrete adhered to the bar.

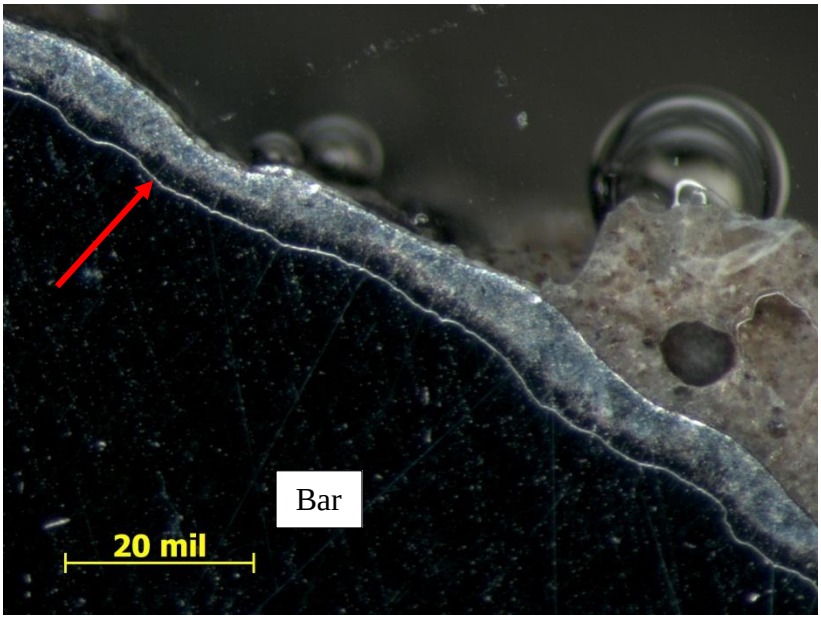

Figure 28. Cross-section of Sample 7, showing the bar (black), the zinc layer (arrow), and small section of concrete adhered to the bar. Epoxy (translucent bubbles), used in the preparation of the cross-section, is also present adhered to the zinc layer.

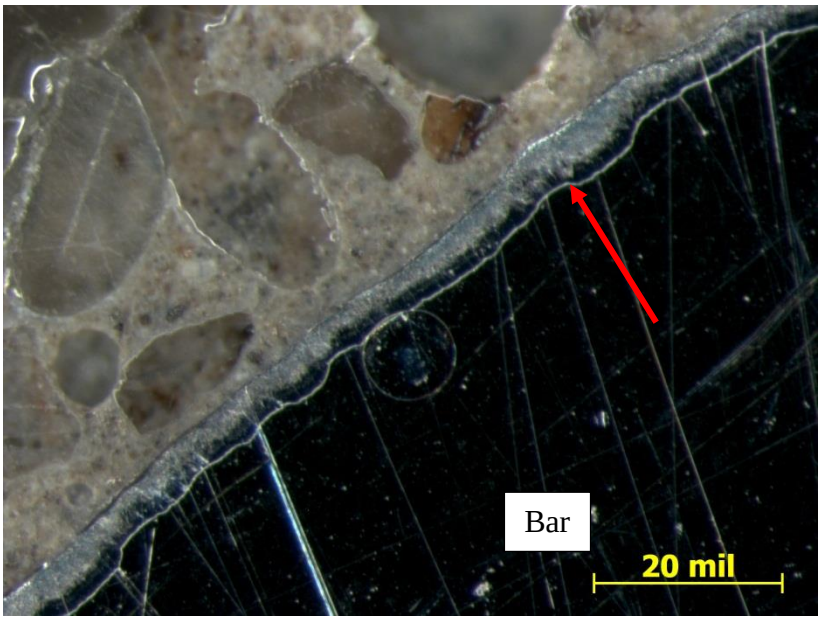

Figure 29. Cross-section of Sample 8, showing the bar (black) and the zinc layer (arrow), and concrete adhered to the bar.

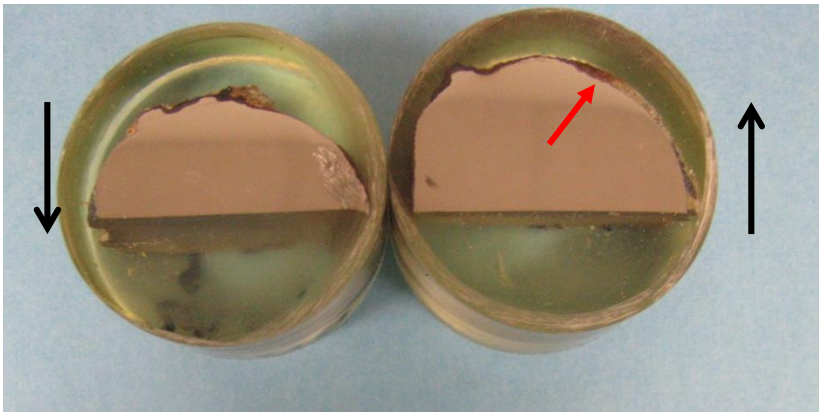

Figure 30. The polished cross-sections of Sample 9. The bar was cut in half so it could be placed into the epoxy molds. Arrows indicate which side was facing up in the slab. Some pitting can be seen on the top surface of the right-hand specimen (red arrow).

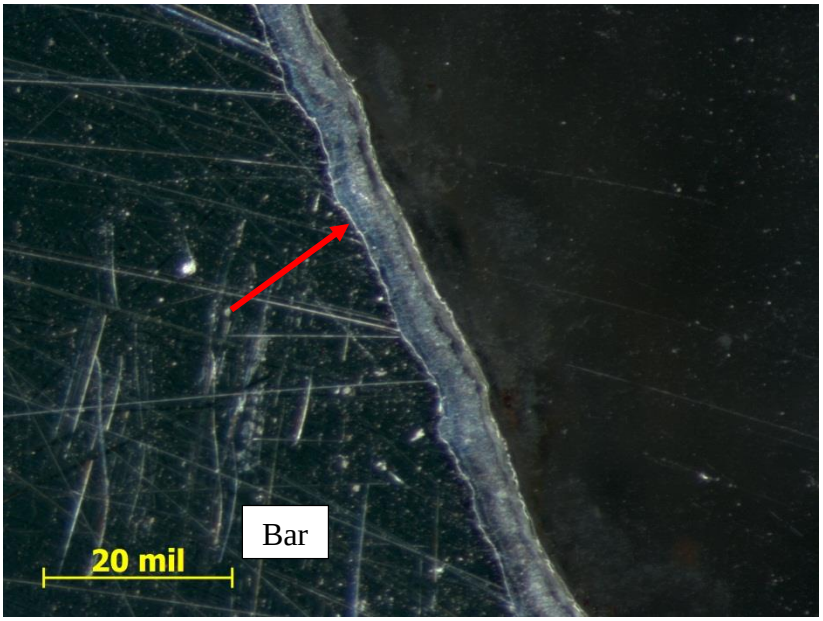

Figure 31. Cross-section of Sample 9, showing the bar and an intact zinc layer (arrow).

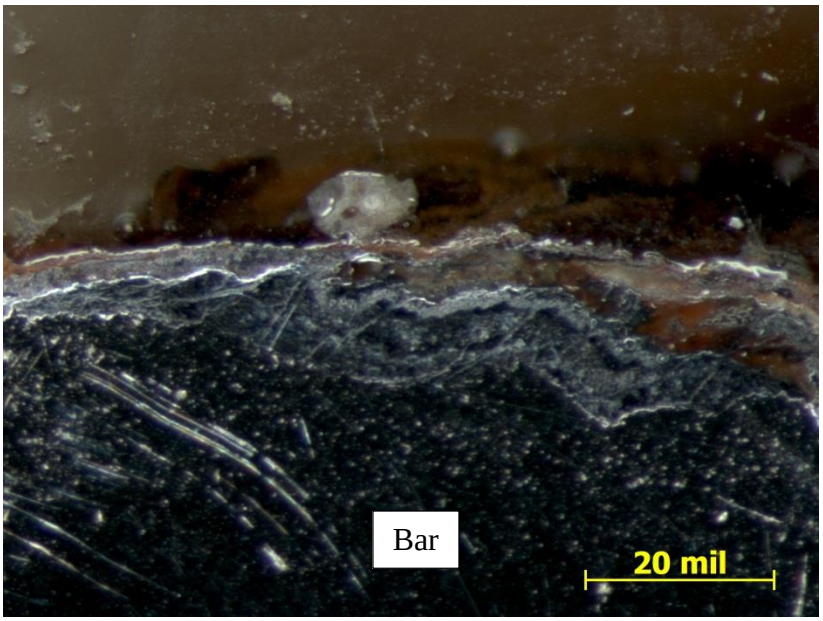

Figure 32. Cross-section of Sample 9, showing corroded bar.

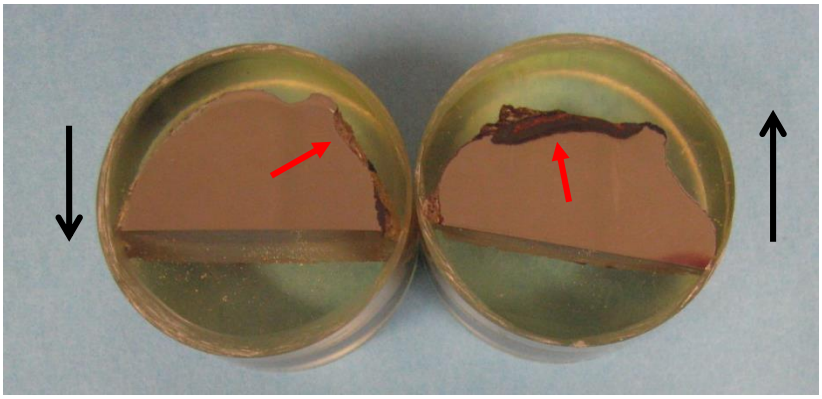

Figure 33. The polished cross-sections of Sample 10. The bar was cut in half so it could be placed into the epoxy molds. Arrows indicate which side was facing up in the slab. Significant pitting can be seen on the top surface of the right-hand specimen, and minor pitting can be seen on the bottom surface (red arrows).

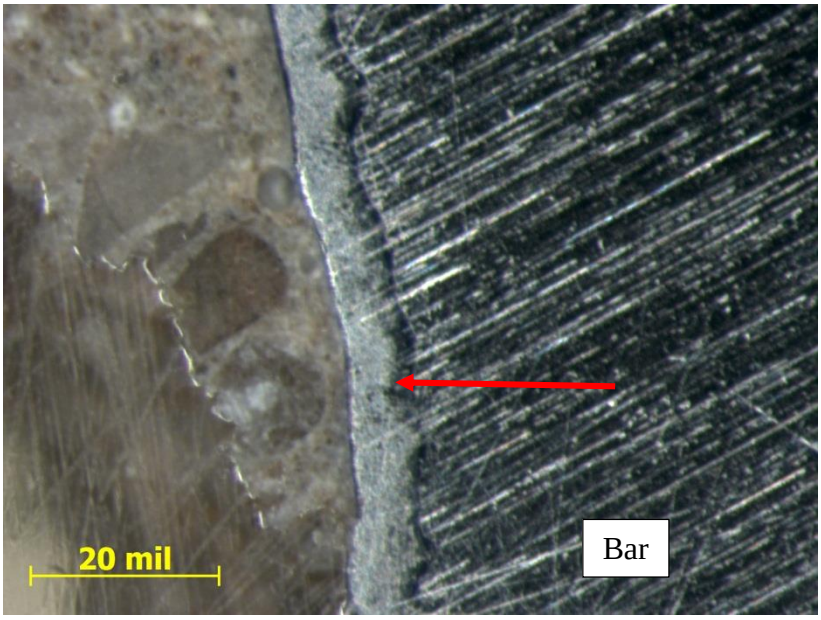

Figure 34. Cross-section of Sample 10, showing the bar, the intact zinc layer (arrow), and concrete adhered to the bar.

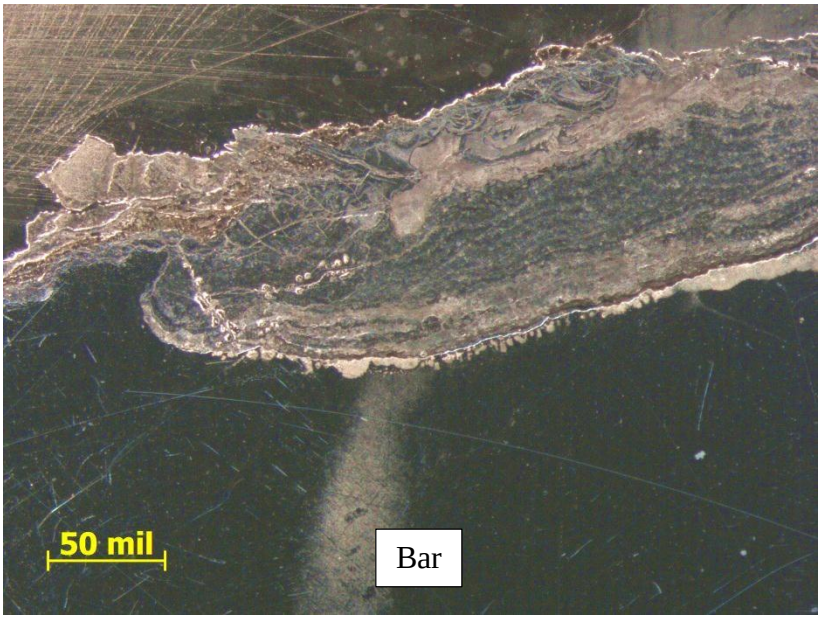

Figure 35. Cross-section of Sample 10, showing the corroded bar and pitting corrosion.

WJE ENGINEERS ARCHITECTS MATERIALS SCIENTISTS

APPENDIX E

Follow-Up Site Visits

WJE ENGINEERS ARCHITECTS MATERIALS SCIENTISTS

Wiss, Janney, Elstner Associates, Inc.
330 Pfingsten Road
Northbrook, Illinois 60062
847.272.7400 tel | 847.291.5189 fax
www.wje.com

APPENDIX E - FOLLOW-UP SITE VISITS

Introduction

As a follow-up to the evaluation of the performance of galvanized reinforcing bars in the bridge deck of Iowa State Highway 92 over Drainage Ditch #25 in western Louisa County, Iowa, John Lawler of Wiss, Janney, Elstner Associates, Inc. (WJE) visited the project site during deck repair operations, which were performed subsequent to our evaluation of this bridge deck. The deck repair work included milling the top surface of the bridge deck, the removal and replacement of concrete at areas of delamination, casting a concrete overlay over the entire bridge deck, and installing new joints. To keep the bridge open to traffic, the repairs to the bridge deck were performed on one-half of the bridge at a time, with the contractor beginning work in the Fall of 2013 on the westbound lanes, and with the eastbound lanes being repaired during the Spring of 2014. As a result, WJE made site visits on October 7, 2013 and April 2, 2014, in both cases after concrete repair work had begun. The objectives of the site visits were to observe repair operations, to inspect the conditions of the bars exposed by the repair process, and to verify that any conditions of distress observed after deck surface milling were consistent with observations of the deck top surface made during the WJE field investigation.

At the time of these visits, the top 1/4-in. of the deck surface had been milled off, the deck had been sounded to identify delaminations, and the delaminations had been removed by chipping, leaving the tops of reinforcing steel exposed. In addition, the concrete surrounding the top mat of reinforcing at the joints had been removed in a strip approximately 2 feet wide. Figures E1 to E4 show representative views of the deck and repair openings in the westbound lanes, while representative views of the deck and repair openings in the eastbound lanes are provided in Figures E5 through E8. Subsequent repair procedures not witnessed by WJE were to include: sandblasting or shotblasting the concrete surface, installation of new joints, and placement of a concrete overlay.

Review of Proposed Coating Repair Materials

Prior to the start of the deck repair work, WJE consulted with the contractor to help them select a material to repair locations of damaged coating on the reinforcing bars exposed at the deck repair openings. IaDOT specifications indicate that a coating should be applied to any bare reinforcing steel exposed during repair of bridge decks with epoxy-coated reinforcing bars, but similar guidance is not provided for galvanized reinforcing. In theory, the galvanizing layer on a reinforcing bar can be restored by using a zinc-based coating, but an epoxy-based product for coating reinforcing bars could also be effective because it would electrically isolate the reinforcing bar in the repair openings. After several communications regarding this topic, it is our understanding that the contractor elected to use a zinc-rich anti-corrosion coating designed for use on reinforcing steel.

Methods

During both site visits, WJE inspected the repair openings, performed a delamination survey by chain drag of the deck surface, and measured the thickness of the galvanizing layer on exposed bars by electromagnetic thickness gauge (Elcometer 456 Coating Thickness Gauge).

Findings and Discussion

Repairs

Most repair openings were generally localized and were directly associated with corrosion of a single reinforcing bar. In a number of cases where two reinforcing bars were exposed during excavation, only one appeared to be actively corroding (see Figure E6). The corrosion was generally associated with cracks that were in-line with the corroded bar (see Figure E9).

The repair excavations at corroding reinforcing bars generally extended only to the top surface of the exposed reinforcing bars, as can be seen in Figures E2, E3, E6, E7, and E8. This location defined the bottom of the delamination and the extent of the "unsound" concrete, so all delaminated concrete was being removed. We understand that the applicable IaDOT specifications give the bridge engineer the responsibility for establishing the depth of repair, stating the following: "Removal for Class A repair extends at least to the level of the top reinforcing bars, and deeper, as determined by the Engineer, to remove unsound concrete." In addition, we understand that the general policy is that if more than half of the bar diameter is exposed, the entire bar should be exposed. Therefore, the amount of concrete removal we observed was consistent with IaDOT specifications and project requirements. Additionally, the extent of concrete removal was generally consistent with the extent of delaminated concrete identified by WJE during the 2012 field investigation.

While the observed repair openings at locations of reinforcing corrosion generally did not expose more than half the bar, we generally recommend that repair of concrete damage due to chloride-driven corrosion should include removal of concrete around the entire perimeter of the bar to at least 3/4 in. below the corroded bar section. This practice is discussed extensively in the literature, including in ICRI 310.1R-2008 *Guideline for Surface Preparation for the Repair of Deteriorated Concrete Resulting from Reinforcing Steel Corrosion*. While removal of concrete below the bars may include removing otherwise sound concrete, the intent is to remove concrete with elevated levels of chloride so as to re-establish passive conditions at the bar by encapsulating the bars in new, uncontaminated repair concrete. This will reduce the risk of corrosion initiating on the bar below the interface with the repair material and increase the life of the repair. Note that this does not address the potential for the ring-anode (or "halo") effect, a process by which corrosion in bars adjacent to concrete repairs is accelerated by locally large differences in the internal concrete environment at the perimeter of patch repairs. However, coating the reinforcing bars exposed in a repair opening with an electrically insulating coating such as an epoxy would reduce the risk of ring-anode corrosion by increasing the resistance path within the repair.

Concrete removal not directly related to corrosion damage had been performed at the ends of the decks and the west approach slab on the eastbound lane apparently to allow for the installation of a new joint seal system. The concrete removal at these repair openings was performed to a depth below the top layer of reinforcing steel, as can be seen in Figure E4. The epoxy coating on the reinforcing exposed in the approach slab was damaged as shown in Figure E10. The contractor indicated that a coating patch material would be applied to the bars prior to concrete installation, as required by IaDOT specifications. Even with this repair, it should be recognized that the protection afforded to the reinforcing steel by the original fusion-bonded epoxy coating has been reduced.

Finally, partial depth concrete removal had also been performed around the deck scuppers (Figure E11), reportedly to accommodate elevation modifications associated with the new overlay. The cover at the drains will be less, somewhat reducing the corrosion protection at this already vulnerable site.

Galvanizing thickness

The results of the galvanizing layer thickness testing are given Table E1. As expected, the thickness of the galvanizing layer varied depending on the level of corrosion of the reinforcing bars. If significant corrosion had occurred, such as shown in Figure E12, less zinc was present and thickness measurements from 0 to 3.9 mils were recorded. However, where no corrosion product was visible, the galvanizing thickness ranged from 5.2 to 8.0 mils. These values are consistent with the thicknesses measured during the 2013 work.

Modeling

A primary component of WJE's 2012 investigation was quantifying the corrosion resistance of the galvanized reinforcing in terms of a corrosion threshold and propagation time, as implemented in a service life model, based on the observed rate of distress development calculated from information available from surveys or repair projects of the bridge deck conducted in 2006 and 2009, and the 2012 WJE survey. To assess the progression of damage between WJE's 2012 deck survey and the recent repairs, WJE identified new deterioration by comparing the repair areas with the results of the 2012 delamination survey of the deck. A combined total of 4.1 sq. ft. of additional delamination was observed during the October 2013 and Spring 2014 site visits, bringing the total estimate of distress up to 131.6 sq. ft., which corresponds to 4.2 percent of the total deck area. While additional damage was observed, the interval between measurements was only one year, so the fact that the increase in damage was small is not surprising.

In Figure E13, this percentage of damage is added to the prior observations of damage and the damage projected through service life modeling that was shown in Figure E13. This new data point falls well within the range of damage projected based on the range of assumed chloride thresholds and propagation times. Therefore, a modification to WJE's quantification of corrosion resistance (ranging from a chloride threshold of 0.095 percent by weight with a propagation time of 18 years to a chloride threshold of 0.188 percent by weight with a propagation time of 5 years) is not warranted based on this information.

Tables

Table E1. Thickness of zinc coating on bars exposed in repair areas

Location	Westbound		Eastbound	
	Thickness (mils)	Steel corrosion product visible?	Thickness (mils)	Steel corrosion product visible?
1	5.9	No	5.8	No
2	5.9	No	6.2	No
3	5.7	No	7.8	No
4	8.0	No	5.2	No
5	5.3	No	3.7	Yes
6	3.9	Yes	2.0	Yes
7	0	Yes	7.3	No
8	7.9	No		
9	7.9	No		

Figures

Figure E1. Overall view of IA92 deck, westbound lanes during Oct. 7, 2013 site visit.

Figure E2. Close-up of typical repair location in IA92 deck, westbound lanes.

Figure E3. Typical repair location in IA 92 deck, westbound lanes

Figure E4. Deeper removal along end joint at westbound lanes

Figure E5. Overall view of IA92 deck, eastbound lanes during April 2, 2014 site visit.

Figure E6. Close-up of repair location in IA92 deck, eastbound lanes.

Figure E7. Typical repair location in IA 92 deck, eastbound lanes.

Figure E8. Deck repair location extending from deeper repair at end joint in eastbound lanes of IA 92 deck.

Figure E9. Corroding bar at crack (yellow line) in eastbound lanes.

Figure E10. Damage to epoxy coating on bars in west approach slab in eastbound lanes

Figure E11. Concrete removal at scupper drain on westbound lane.

Figure E12. Close-up of corroded bar in westbound lanes.

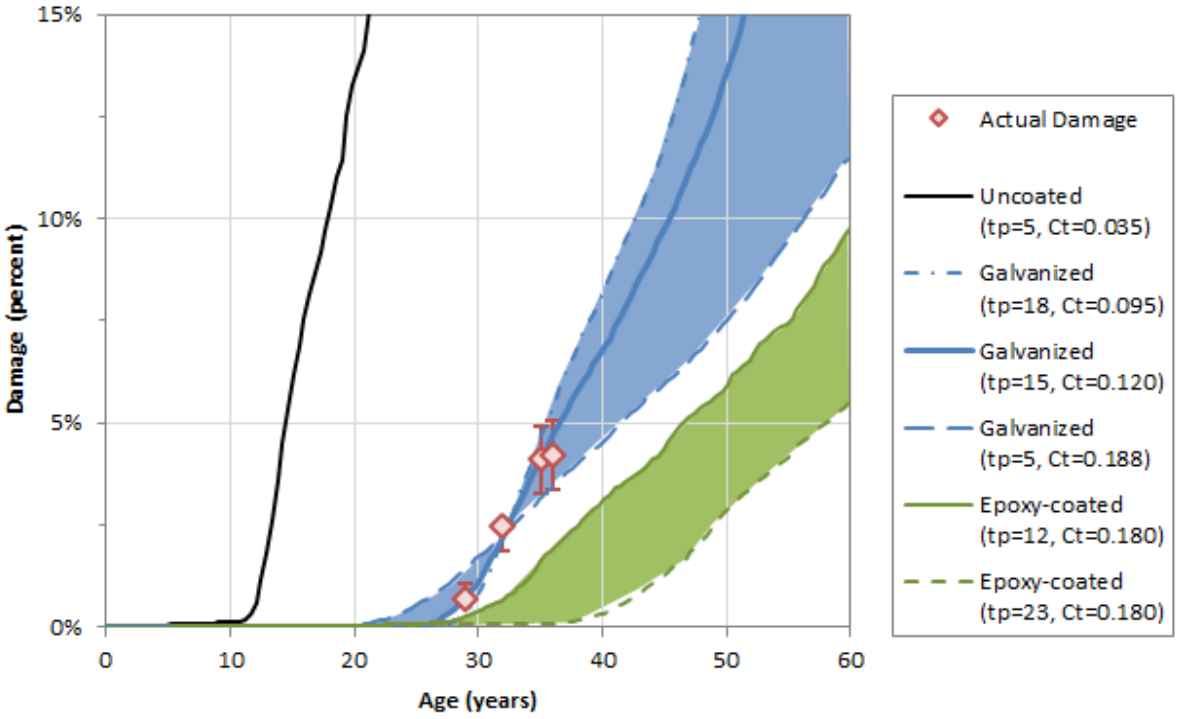

Figure E13. Results of service life model for bridge - updated to show additional distress through 2013/2014. (Propagation time (tp) is given in years, and chloride threshold (Ct) is given in percent by weight of concrete.)